Adv. Stat. Clim. Meteorol. Oceanogr., 12, 275–303, 2026
https://doi.org/10.5194/ascmo-12-275-2026
© Author(s) 2026. This work is distributed under
the Creative Commons Attribution 4.0 License.

ASCMO
Open Access

Analyzing temporal dependence between extreme events using point processes

Antoine Heranval[1], **Denis Allard**[1,★], **Edith Gabriel**[1,★], **and Thomas Opitz**[1,★]

[1]Biostatistiques et Processus Spatiaux (BioSP), INRAE, Avignon, France
★These authors contributed equally to this work.

Correspondence: Antoine Heranval (antoine.heranval@inrae.fr)

Received: 19 February 2026 – Revised: 20 October 2026 – Accepted: 21 October 2026 – Published: 9 November 2026

Abstract. Extreme meteorological events often occur in complex temporal configurations, where the impacts of one hazard may depend on the prior occurrence of others. Characterising such temporal dependencies is essential for understanding compound climate risks, yet remains challenging due to the discrete, heterogeneous, and clustered nature of extreme events. In this study, we extend and apply temporal point process methods to characterise dependencies among extreme meteorological events occurring within appropriately defined spatial regions across Europe, focusing exclusively on their temporal structure.

We introduce an event-based framework in which extreme events are represented as marked temporal point processes, with marks describing key characteristics such as intensity or duration. Global first- and second-order temporal statistics are used to quantify clustering, co-occurrence, and directional dependencies between different types of extremes. We rely on directional cross-K functions to assess whether the occurrence of one type of extreme event systematically modifies the short-term probability of subsequent events of another type.

Two complementary applications illustrate different facets of compound event analysis. First, we demonstrate the relevance of the framework for preconditioned or cascading compound events through a temporal analysis of wildfire-related meteorological extremes. Second, we examine temporal dependence between extreme precipitation, extreme wind, and extreme atmospheric instability across all European NUTS-2 regions.

Building on these second-order statistics, we develop formal tests of temporal independence to assess the significance of observed directional interactions between different types of extreme events. Overall, this temporal point process framework provides a rigorous and interpretable approach to the analysis of compound climate extremes, with direct applications to climate risk assessment and early-warning systems.

1 Introduction

The climate system exhibits complex behaviour arising from interactions among numerous processes operating across multiple spatial and temporal scales. Understanding and modelling extreme climate phenomena and their impacts therefore requires analysing not only their frequency and magnitude, but also their temporal clustering, spatial extent, and interdependencies. Extreme weather events – such as intense precipitation, destructive winds, severe convective storms, and wildfires – pose substantial risks to society, infrastructure, and ecosystems. Importantly, the most severe impacts often arise not from isolated extremes, but from compound events, in which multiple hazards co-occur or interact in time and space, for example when one extreme event amplifies the impacts of other subsequent events (Leonard et al., 2014; Zscheischler et al., 2020).

Compound extreme events can take various forms, some of which are particularly relevant for climate risk assessment:

- *Multivariate compound events*, involving multiple risk drivers or hazards, occurring simultaneously or in rapid succession, such as convective storms, including hail, producing both extreme precipitation and damaging surface winds under high atmospheric instability.

- *Preconditioned compound events*, where one extreme event creates conditions that amplify the impacts of subsequent events, for example when prolonged heat and drought create highly fire-prone conditions (as quantified by indices such as the Fire Weather Index, FWI) favouring wildfire ignition. This type of events may also be referred to as cascading compound events, especially when the preconditioning event alone already presents a hazard or risk; see also Moddemeyer et al. (2022).
- *Temporally compounding events*, characterised by sequences of similar extremes occurring within short periods, preventing recovery between impacts, such as consecutive heat waves or clustered storm systems.
- *Spatially compounding events*, involving concurrent or closely timed extremes across multiple regions, often driven by large-scale atmospheric circulation patterns.

Despite their importance, compound extremes remain challenging to characterise and model. Traditional climate analyses often focus on individual variables (e.g. daily maximum temperature or precipitation totals) and rely on statistical methods that implicitly assume independence between events or processes. In contrast, the physical mechanisms governing extreme weather are inherently multivariate and interactive, as highlighted by the following examples. Atmospheric instability, quantified by indices such as Convective Available Potential Energy (CAPE), provides the thermodynamic conditions for severe convection, which can manifest as both extreme precipitation and surface wind hazards. Synoptic-scale circulation patterns drive spatially coherent extremes affecting multiple regions simultaneously or in rapid succession. Fire weather conditions integrate temperature, humidity, wind, and antecedent precipitation, characterising temporal windows during which ignitions are more likely and more often develop into large and damaging wildfires.

Analysing such dependencies poses several statistical challenges. Modern reanalysis products such as ERA5 provide gridded data at fine spatial (0.25°) and temporal (hourly) resolutions, resulting in high-dimensional datasets with millions of data points. Extreme events can exhibit pronounced spatial and temporal clustering, violating independence assumptions underlying many classical statistical approaches. Moreover, compound event analysis may require the joint treatment of multiple meteorological variables with different physical units, marginal distributions, and characteristic time scales, see Jacquemin et al. (2026) for an example. Finally, ongoing climate change is modifying the frequency, intensity, and co-occurrence of extremes, calling for methods that can capture short-term interactions while remaining robust to long-term nonstationarity.

Here, we focus on point process methods (Kingman, 1992; Daley and Vere-Jones, 2003) since they offer a natural and flexible event-focused framework for addressing these challenges. Rather than analysing continuous time series or gridded fields directly, point process approaches can be used to represent extreme events as discrete occurrences in time and space, explicitly focusing on event timing, clustering, and interactions. In marked point processes, marks can be attached to points to indicate relevant numerical variables associated with each event, such as its magnitude or duration. In extreme-value theory, certain point processes arising asymptotically for exceedances above high thresholds were characterized in early papers (Pickands III, 1971; Hsing et al., 1988). By extracting only sparse data representing the key properties of relevant events from large databases, point processes allow for a strong reduction of data volumes, processing and storage costs for statistical analyses. This event-based perspective aligns closely with risk assessment objectives, where questions regarding the likelihood of multiple hazards occurring within operational time windows (days to weeks) or across multiple regions are of central importance. Fundamental characteristics of point processes are their first-order and second-order behaviour. Regarding first-order behaviour, the intensity function describes the mean arrival rate, which can vary over time. Second-order behaviour is related to local pairwise interactions between points, such as repulsion or clustering, and can be described with tools such as Ripley's K-function (Ripley, 1976).

In this study, we apply point process methods to characterise temporal dependencies among extreme meteorological events occurring in appropriately chosen spatial regions across Europe, focusing on two complementary applications that illustrate different facets of compound event analysis. First, we demonstrate the framework's relevance for preconditioned compound events through a local analysis of wildfire-related weather conditions and their extremes, using local cross-K functions to quantify how the combination of antecedent weather events creates short-term windows of elevated wildfire risk. Then, we examine multivariate compound events by analysing temporal clustering between extreme precipitation, wind, and atmospheric instability (CAPE) within individual regions, and we investigate spatially compounding events by comparing temporal dependencies across geographically distinct regions, thereby identifying the spatial scales over which extremes tend to cluster. Together, these applications illustrate how point process methods enable a rigorous, event-based formal characterisation and visual representation of compound climate extremes that goes beyond traditional analyses based on correlations between continuous variables and can provide valuable complementary information.

1.1 Data

All analyses presented in this study are based on meteorological data derived from the ERA5 reanalysis (Hersbach et al., 2023), produced by the European Centre for Medium-Range Weather Forecasts (ECMWF) and distributed through

the Copernicus Climate Data Store. ERA5 provides spatially and temporally consistent estimates of atmospheric variables by combining numerical weather prediction models with a wide range of observational data. Relying on a single reanalysis product ensures internal consistency across variables and regions, which is essential for the comparative analysis of multivariate extreme events.

ERA5 offers global coverage at a native spatial resolution of 0.25° and an hourly temporal resolution. In this study, all variables are aggregated to daily values, corresponding to the temporal scale at which extreme events are identified and analysed. Depending on the application, the same underlying ERA5 fields are used to construct datasets at different spatial scales. Some analyses focus on a limited number of selected regions to investigate detailed fire weather dynamics, while others are conducted systematically across all European NUTS-2 regions to characterise large-scale spatial patterns of temporal dependence. Despite these differences in spatial aggregation, all datasets originate from the same ERA5 reanalysis, ensuring methodological coherence.

Two partially overlapping temporal domains are considered. For the continental-scale analysis of dynamical and convective extremes, we use the full ERA5 record from 1941 to 2024, which allows long-term variability and rare extreme events to be examined within a homogeneous data framework. This extended period is particularly well suited for analysing extreme precipitation, wind, and atmospheric instability at the European scale.

In contrast, the analysis of fire weather conditions based on the Fire Weather Index (FWI) is restricted to the period 2000–2022. FWI is used as an integrated indicator of fire danger, synthesising information on fuel moisture, atmospheric dryness, and wind effects. In addition to FWI, several meteorological variables known to influence fire behaviour are considered, including near-surface air temperature, relative humidity, wind speed, incoming shortwave radiation, precipitation, and vapour pressure deficit (VPD).

For the continental-scale application, we extract daily fields of total precipitation, near-surface wind speed, and Convective Available Potential Energy (CAPE) from ERA5. Together, these variables provide a consistent and comprehensive basis for investigating temporal interactions between different types of meteorological extreme events across Europe.

1.2 Objectives and Contributions

The primary objective of this study is to develop and apply an event-based statistical framework for characterising temporal dependence between different types of meteorological extreme events across Europe. The central idea is to first construct physically interpretable spatio-temporal event catalogues from gridded extreme data points and then represent these events and their properties using marked temporal point processes. This representation allows us to investigate interactions between extreme events while overcoming limitations of approaches based on individual grid-cell exceedances or restrictive temporal independence assumptions.

We focus on short-term temporal interactions between extremes, with particular emphasis on cascading and compound events, where the occurrence of one type of extreme may modify the likelihood of subsequent events. By analysing dependence at the event level rather than at the level of isolated spatial points, the proposed framework provides an interpretable description of how extreme events interact in time while retaining information on their characteristics, including magnitude, duration, and spatial footprint.

Two complementary applications are used to illustrate different facets of compound event analysis. The first application focuses on wildfire-related extremes and investigates preconditioning mechanisms leading to elevated fire danger. Extreme fire weather conditions are represented using the Fire Weather Index (FWI), and temporal interactions with extremes of other meteorological variables are analysed in three contrasted regions of southern and south-western Europe. This regional-scale analysis aims to identify systematic short-term temporal associations between FWI extremes and concurrent or antecedent meteorological conditions, while accounting for strong seasonality and interannual variability.

The second application adopts a continental-scale perspective and examines temporal dependence between extreme precipitation, extreme wind, and extreme atmospheric instability across all European NUTS-2 regions. Using a common statistical framework applied uniformly across regions, we first assess temporal dependence patterns at the regional level and then investigate their spatial organisation across Europe. Particular attention is given to interactions between variables, with the objective of determining whether extreme CAPE events systematically precede subsequent extreme precipitation or wind events.

The main contributions of this work are threefold. First, we introduce an event-based point-process framework that links spatio-temporal clustering of extremes with marked temporal dependence analysis, providing a unified representation of compound extreme events. Second, we develop a coherent statistical framework for testing the null hypothesis of temporal independence in inhomogeneous temporal point processes exhibiting strong seasonal structure, and we compare different simulation-based null models to clarify the interpretation of temporal dependence under different assumptions on the first-order intensity. Third, through two contrasted applications – one focused on fire-weather preconditioning at the regional scale and one addressing convective and dynamical extremes at the continental scale we demonstrate the flexibility of the framework for analysing climate-related event interactions. One of the main objectives of this study is to show that the proposed point-process representation provides more than a computational simplification; it also offers a conceptual advantage. By transforming high-dimensional gridded extremes into an event catalogue with interpretable

marks, it facilitates the analysis of dependence structures at the event level.

An open-source implementation in R is provided to ensure full reproducibility and to facilitate the application of these methods to other climate-related and environmental event datasets.

1.3 Structure of the Paper

The remainder of this paper is organised as follows. Section 2 describes the construction of the extreme event catalogues, including the definition of thresholds and event identification. Section 3 introduces the temporal point process framework and the second-order statistics used to characterise temporal dependence between extreme events.

The simulation-based testing framework for assessing temporal independence, including the different null models considered, is presented in Sect. 4. Section 5 applies the proposed methodology to wildfire-related extremes, focusing on temporal preconditioning mechanisms involving the Fire Weather Index in three Mediterranean regions.

A continental-scale application investigating temporal interactions between extreme meteorological events across Europe is presented in Sect. 6, with particular attention to extreme precipitation, wind, and atmospheric instability. Finally, Sect. 7 discusses the main results, methodological limitations, and implications for compound risk assessment, and outlines perspectives for future research.

2 Construction of Extreme Event Catalogues

Identifying and characterising meteorological extremes is a central task in climate analysis, hazard assessment, and impact modelling. Extreme events such as heavy precipitation, heatwaves, or strong winds are typically defined as realisations that deviate substantially from the bulk of the distribution of the underlying meteorological variable. Classical extreme value theory (EVT) distinguishes between block-maxima approaches based on the Generalised Extreme Value (GEV) distribution (Coles, 2001) and threshold-based approaches such as the Peaks-Over-Threshold (POT) framework, which models exceedances above a high threshold using the Generalised Pareto distribution (Davison and Smith, 1990; Pickands, 1975).

POT-based approaches are theoretically well founded and have been extensively applied in the climate sciences (Coles, 2001). However, their direct implementation can become challenging when dealing with large gridded datasets comprising tens of thousands of locations. In such contexts, two practical issues commonly arise. First, threshold selection must be carried out independently at each grid point, and classical diagnostic tools (e.g. mean residual life plots or parameter stability plots) are difficult to automate and scale. Second, strong spatial nonstationarity implies that a single global threshold is rarely appropriate, as climatological regimes vary substantially across regions due to differences in topography, latitude, and proximity to moisture sources.

A commonly adopted and closely related strategy in climatology is to define extremes as exceedances of high empirical quantiles of the local climatological distribution (e.g. the 95th or 99th percentile). From a conceptual perspective, this approach can be viewed as a practical variant of the POT framework, in which the threshold is specified empirically rather than through parametric tail modelling. By allowing the threshold to adapt to local climate conditions, this strategy facilitates consistent comparisons across regions while avoiding the need to fit a separate tail model at each grid point.

A further complication is that meteorological extremes often exhibit pronounced spatio-temporal dependence. For example, extreme precipitation events tend to cluster in time and space due to the persistence of synoptic-scale weather systems, thereby violating the independence assumptions underlying classical EVT. Diagnostic tools such as the extremal index or the extremogram (Davis and Mikosch, 2009, 2013) provide a useful preliminary characterisation of this dependence structure. Extremograms, which may be viewed as correlation functions adapted to extreme events, indicate the temporal or spatial lags over which exceedances remain dependent and can therefore inform the definition of composite events or the choice of minimum separation times and distances.

In this study, extreme events are defined as local exceedances of high empirical quantiles, applied independently at each grid point. This choice remains fully consistent with the POT paradigm, while emphasising a point-process representation of exceedances that is well suited to large-scale gridded datasets. Compound events are subsequently analysed through the spatio-temporal interaction and co-occurrence of these exceedances, either across different variables or through clustering in space and time. This perspective enables a flexible analysis of dependence structures while retaining a clear conceptual link with threshold-based EVT.

2.1 Threshold Selection

Extreme events are defined as exceedances of high percentiles of the climatological distribution. For each variable, a high quantile (q_p) of daily values is computed over the entire available period, separately for each grid point. Using local thresholds estimated over a long reference period provides a stable and consistent definition of extremeness that is particularly relevant from an impact and risk perspective since extreme events are defined as strong anomalies with respect to the common local weather conditions. This approach targets rare values that are associated with potentially severe consequences and substantial damage, and is therefore well aligned with applications in climate risk assessment and insurance-related analyses.

Formally, for a variable X at grid point ℓ, and at time t (a day) within the total period T, the threshold is defined as:

$$\tau_\ell = \text{quantile}_p\left(\{X_{\ell,t} : t \in T\}\right). \quad (1)$$

An exceedance occurs when $X_{\ell,t} > \tau_\ell$, and its magnitude is defined as $m_{\ell,t} = X_{\ell,t} - \tau_\ell$. The quantile level p is variable-specific and selected to isolate rare and high-impact events.

A key issue when defining such thresholds is the seasonal nonstationarity of the underlying climatic processes. As will be seen later in Sect. 3, seasonal nonstationarity can be accounted for using a transformation of the cumulative time-varying intensity function $\lambda(t)$.

By contrast, if one were to rely on a classical autocorrelation function (ACF), substantial pre-processing would be required. In particular, the original variables would first need to be deseasonalised in order to obtain meaningful results. Such preprocessing steps can be considerably more complex, as nonstationarity may affect not only the mean, but also the variance and/or the tail behaviour of the distribution. Consequently, the PP approach provides a more flexible and parsimonious framework for analysing extreme events in the presence of temporal nonstationarity.

2.2 Spatio-Temporal Declustering

Raw threshold exceedances do not directly correspond to impactful meteorological events, which often extend over multiple grid cells and persist for several days. To construct coherent events, we apply connected-component analysis in the spatio-temporal domain within each region of interest.

Two exceedances at space–time coordinates (ℓ_1, t_1) and (ℓ_2, t_2) within the same region are considered connected if they are sufficiently close both in space and time, according to application-specific spatial and temporal thresholds:

$$d_{\text{space}}(\ell_1, \ell_2) \le \delta_{\text{space}} \quad \text{and} \quad d_{\text{time}}(t_1, t_2) \le \delta_{\text{time}}, \quad (2)$$

where δ_{space} and δ_{time} denote user-defined spatial and temporal connectivity parameters.

The spatial distance d_{space} is computed as the Euclidean distance between event locations after projecting geographic coordinates (longitude, latitude) into a metric coordinate reference system (ETRS89/LAEA Europe, EPSG:3035), ensuring distances are expressed in meters. The temporal distance d_{time} corresponds to the gap (in days) between the temporal intervals of two exceedance events, allowing for a limited temporal separation between consecutive events.

We construct an undirected graph in which nodes represent individual exceedances (grid point × day), and edges connect exceedances that satisfy the connectivity criterion (2). Each connected component of this graph defines a discrete extreme event e and is characterized by its properties:

- *Start date* t_e^{start}: earliest day with an exceedance in the cluster;
- *End date* t_e^{end}: latest day with an exceedance;
- *Duration* $\Delta t_e = t_e^{\text{end}} - t_e^{\text{start}} + 1$;
- *Total magnitude* $M_e = \sum_{(\ell,t)\in e} m_{\ell,t}$: sum of excesses at all space-time locations affected by the event.

Figure 1 illustrates how local threshold exceedances are aggregated and declustered into discrete events, which subsequently define the temporal point process. For this analysis (Sect. 3), each spatio-temporal event is reduced to a single time point, $t = t_e^{\text{start}}$, representing the event onset. This simplification is appropriate for testing temporal independence, as the focus lies on the timing of event occurrences rather than on their full spatio-temporal evolution. Each event therefore corresponds to a single point in the resulting point process, enabling the use of standard tools from point process theory to analyse the temporal structure of extreme events.

We note that representing each spatio-temporal event by its onset time may shift the apparent lead times for long-lasting episodes. In particular, when events persist over several days, a directional association should be interpreted as an ordering between onsets rather than between complete episodes. Alternative representatives, such as the event midpoint or peak day, may be considered in sensitivity analyses.

3 Point Processes

In this work, we adopt a marked point process framework to represent extreme meteorological events as discrete, stochastic occurrences in time (Daley and Vere-Jones, 2003; Diggle, 2013). Within this paradigm, extreme events are formalized as points located in a temporal domain, each carrying associated marks – numerical attributes such as intensity (e.g. precipitation amount, wind speed), duration, or other event-specific metrics – along with a joint distribution of those marks. By operating directly on discrete extreme events rather than on continuous time series or gridded climate fields, this framework naturally aligns with impact-based perspectives and is particularly well suited to large-scale applications, as it relies on sparse event representations and avoids processing full high-resolution gridded datasets.

Point process approaches have been successfully applied in related domains, notably to model wildfire occurrence and spread (Peng et al., 2005; Gabriel et al., 2017; Xi et al., 2019; Koh et al., 2023). In the context of meteorological extremes, several studies have explored the use of K-functions to investigate clustering and dependence structures (Barton et al., 2016; Tuel and Martius, 2022, 2021b, a), primarily focusing on single-variable extremes or bivariate settings within limited regions or time periods. To our knowledge, only a limited number of studies have employed second-order point process statistics to advance the understanding of compound environmental extremes. Sharma and Mujumdar (2024) investigated the spatial synchrony of streamflow droughts using a multivariate Ripley's K-function, while Toreti et al. (2019) anal-

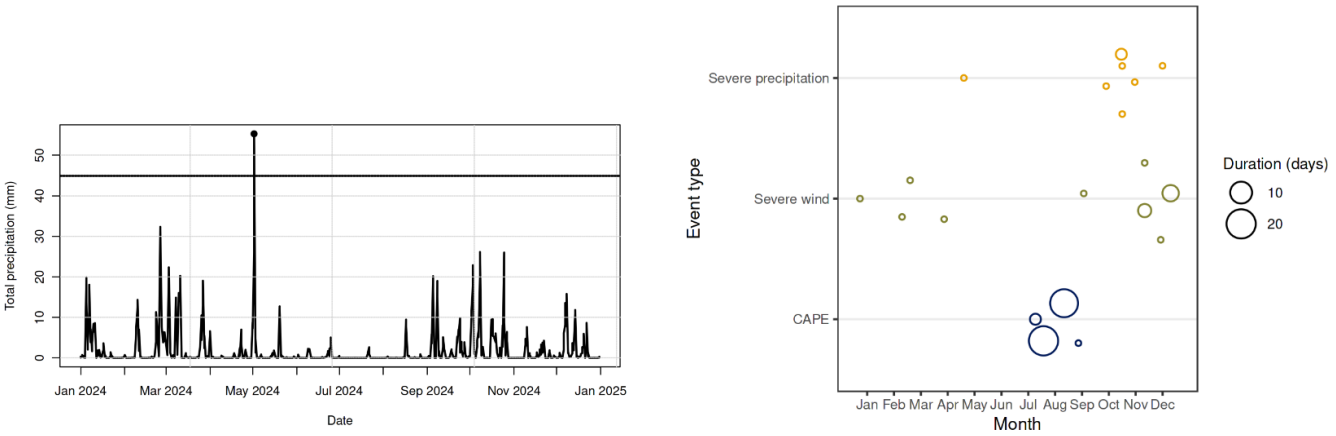


Figure 1. Illustration of the extreme-event construction procedure for NUTS FRL0 in 2024 (subset shown for clarity). Extreme precipitation (in mm) is first identified at each grid point as exceedances of a local high-quantile threshold (left display). These exceedances are then aggregated in space and time and declustered to form coherent events, represented as points in the event calendar (right display). The prominent spring exceedance in the time series is part of one of the detected events in the right display, whereas other late-year precipitation events correspond to exceedances occurring at other grid points within the region.

ysed concurrent climate extremes in major wheat-producing regions using point process methods based on the J-function, incorporating a spatial perspective on event interactions. The application of cross-type K-functions – and in particular directional variants – to compound and preconditioned climate extremes remains a relatively recent and underexplored area of research.

Here, we focus on compound events arising from the temporal clustering of extreme meteorological events. By adopting an event-based representation, compound and preconditioned extremes can be analysed using second-order temporal statistics that explicitly capture inter-event interactions.

3.1 Intensity function and Ripley's K-Function

A point process is characterised by its intensity function $\lambda(t)$, which describes the expected instantaneous rate of event occurrence at time t:

$$\lambda(t) = \lim_{\Delta t \to 0} \frac{\mathbb{E}[N([t, t+\Delta t])]}{\Delta t}. \tag{3}$$

For a stationary process over a window of length T, this reduces to the global intensity $\lambda = \mathbb{E}[N([0,T])]/T$, i.e. the expected number of events per unit time.

In many environmental applications, $\lambda(t)$ varies due to strong seasonal cycles, making a stationary assumption inappropriate. Rather than modelling $\lambda(t)$ over the full temporal domain, we represent the intensity as a periodic function of the normalised day of year $u \in [0,1)$, mapping each event time t_i to its fractional position within the annual cycle. We estimate $\lambda(u)$ via kernel density estimation on the circular domain:

$$\hat{\lambda}(u) = \overline{n}\, \hat{f}(u), \tag{4}$$

where $\hat{f}(u)$ is the kernel density estimate of the day-of-year distribution and $\overline{n} = n/Y$ is the mean annual event count (n total events over Y years). This ensures $\int_0^1 \hat{\lambda}(u)\,\mathrm{d}u \approx \overline{n}$, consistent with a periodic intensity. To avoid boundary artefacts, the kernel estimator is computed on an extended domain by replicating the data outside $[0,1)$. When the number of events is very small, we fall back to a homogeneous Poisson approximation with constant intensity $\hat{\lambda}(u) = \overline{n}$.

The second-order structure of a point process is summarised by Ripley's K-function (Ripley, 1976), which counts events within a temporal neighbourhood of a typical event and compares this count to the expectation under a Poisson null (no interaction). For an inhomogeneous process with intensity $\lambda(t)$, the estimator reweights neighbouring events by the inverse of the local intensity:

$$\hat{K}(r) = \frac{1}{T_{\mathrm{tot}}} \sum_{t_i} \sum_{t_j \neq t_i} \frac{\mathbf{1}\big(|t_i - t_j| \le r\big)}{\lambda(t_i)\,\lambda(t_j)}, \tag{5}$$

thereby isolating genuine second-order dependence from first-order seasonal variation. Under the inhomogeneous Poisson null, $\mathbb{E}[\hat{K}(r)] = 2r$; values above this threshold indicate temporal clustering ($K(r) > 2r$), while values below indicate regularity ($K(r) < 2r$). This inhomogeneous formulation is the foundation for the cross-type extensions described below.

3.2 Cross-type K-function for compound events

To assess temporal dependence between two distinct types of extreme events, we employ cross-type K-functions following the general framework of Cebrián and Asín (2021). While our implementation is conceptually related to the inhomogeneous cross-K available in the `IndTestPP` pack-

age (Cebrián and Asín, 2021), we introduce two key adaptations motivated by the structure of climate time series: a seasonally varying intensity estimated on the day of year, and a directional formulation of temporal dependence.

Let N_x and N_y denote two temporal point processes observed over N_{year} calendar years, with T denoting the number of days per year and $T_{\text{tot}} = N_{\text{year}}\,T$ the total observation period. Event times are embedded on a continuous axis $t = (y-1)T + \text{DOY}$, and temporal distances are computed as $d(t_i, s_j) = |t_i - s_j|$ (or using periodic boundary conditions when appropriate as $d(t_i, s_j) = \min\big(|t_i - s_j|,\ T_{\text{tot}} - |t_i - s_j|\big)$). The seasonal intensities $\lambda_x(u)$ and $\lambda_y(u)$ are estimated separately for each process as described in Sect. 3.1.

The inhomogeneous symmetric cross-K function measures the expected number of type-y events within temporal distance r of a typical type-x event, after removing first-order seasonal variation from both processes the empirical cross-K estimator is defined as:

$$\hat{K}_{xy}(r) = \frac{1}{T_{\text{tot}}} \sum_{t_i \in N_x} \sum_{s_j \in N_y} \frac{\mathbf{1}\big(d(t_i, s_j) \le r\big)}{\hat{\lambda}_x(u_i)\,\hat{\lambda}_y(u_j)}. \tag{6}$$

Under the null hypothesis of independence between N_x and N_y, with an inhomogeneous Poisson structure, $\mathbb{E}[\hat{K}_{xy}(r)] = 2r$. Departures above this reference indicate co-occurrence of the two event types at lag r, a hallmark of compound behaviour. In the homogeneous case, $\hat{\lambda}_x(u_i)$ and $\hat{\lambda}_y(u_j)$ are replaced by their (constant) global values.

A key methodological contribution of this work is the use of a directional (or one-sided) cross-K function, which distinguishes whether type-x events tend to precede type-y events rather than merely co-occurring symmetrically:

$$\hat{K}_{x\to y}(r) = \frac{1}{T_{\text{tot}}} \sum_{t_i \in N_x} \sum_{s_j \in N_y} \frac{\mathbf{1}\big(0 \le s_j - t_i \le r\big)}{\hat{\lambda}_x(u_i)\,\hat{\lambda}_y(u_j)}. \tag{7}$$

Under independence, $\mathbb{E}[\hat{K}_{x\to y}(r)] = r$. Exceedance of this reference at lag r indicates that type-y events are more likely to follow a type-x event within r days than expected by chance, revealing a directional preconditioning relationship. This asymmetry – absent from univariate K-functions and from the symmetric cross-K – is essential for distinguishing preconditioned or cascading compound sequences from mere simultaneous co-occurrence.

Both estimators are evaluated at lags $r \in \{1, 2, \ldots, r_{\max}\}$ (or at half-day increments $r = k + 0.5$), consistent with the daily sampling resolution of the data. Note that $\hat{\lambda}(u)$ in Eqs. (6) and (7) denotes the daily intensity, i.e. $\hat{\lambda}(u)/T$ where T is the number of days per year.

4 Testing Independence via Simulation

Having established a point-process representation of extreme events, we now turn to the assessment of dependence between two event processes. Our objective is to determine whether the observed temporal association between two types of extremes exceeds what would be expected under independence, formalized as

$$H_0 :\ N_x \perp\!\!\!\perp N_y,$$

conditional on their respective intensity functions $\lambda_x(t)$ and $\lambda_y(t)$. Departures from H_0 indicate second-order temporal interactions – clustering, inhibition, or directional precedence – characterised through deviations of the observed cross-type K-functions from their expectations under H_0.

The test is conducted via Monte Carlo simulation: one process (N_y) is resampled under H_0 while the other (N_x) is kept fixed. This asymmetric scheme preserves the observed realisation of N_x and assesses dependence by comparing the observed cross-K function to its simulated distribution under H_0. We embed these summary statistics within the Global Envelope Test (GET) framework (Myllymäki et al., 2017) to perform formal hypothesis testing, controlling the family-wise error rate across all temporal lags. We consider two complementary simulation strategies, described below.

4.1 Simulation strategies

4.1.1 Translation method (Lotwick–Silverman)

We employ a translation-based null model following Lotwick and Silverman (1982), also used in Cebrián et al. (2020). A random temporal shift is applied to N_y while N_x is kept fixed. The shift is drawn uniformly with wrap-around, preserving all first- and second-order properties internal to N_y (event count, inter-event intervals, clustering) while removing any systematic alignment with N_x.

Because seasonality is central to our analysis, translations are applied on the annual cycle using the normalised day-of-year coordinate $u \in [0, 1)$. For each year y, a random shift $\Delta_y \sim \mathcal{U}(0, 1)$ is drawn and the transformed event times are

$$u'_j = (u_j + \Delta_y) \bmod 1, \tag{8}$$

for all events $s_j \in N_y$ in year y. After translation, DOY coordinates are mapped back to the continuous time scale used for cross-K computation.

In the inhomogeneous case, the translation is performed in the rescaled domain defined by the cumulative intensity function to preserve the seasonal first-order structure. Let

$$F(u) = \frac{\int_0^u \hat{\lambda}_y(v)\,\mathrm{d}v}{\int_0^1 \hat{\lambda}_y(v)\,\mathrm{d}v}$$

denote the normalised cumulative seasonal intensity. Each event time u_j is mapped to the uniformised coordinate $z_j = F(u_j)$, the shift is applied as $z'_j = (z_j + \Delta_y) \bmod 1$, and the translated time is recovered by inversion $u'_j = F^{-1}(z'_j)$. This intensity-preserving translation destroys any systematic alignment between N_x and N_y while leaving the seasonal intensity profile of N_y unchanged by construction. Because the

intensity function is used solely to normalise the cross-K estimator rather than to generate events, the procedure is robust to moderate intensity misspecification, making it well suited for systematic comparisons across regions in the presence of strong seasonal nonstationarity.

4.1.2 inhomogeneous Poisson process (IPP)

As a complementary strategy, we resimulate N_y from an inhomogeneous Poisson process with seasonal intensity $\hat{\lambda}_y(u)$ estimated as in Eq. (4). Simulations are performed independently for each calendar year using a thinning algorithm (Lewis and Shedler, 1979):

1. Compute $\lambda_{\max} = \max_{u\in[0,1)} \hat{\lambda}_y(u)$;
2. Generate $n_{\text{cand}} \sim \text{Poisson}(\lambda_{\max})$ candidate times uniformly over $[0, 1)$;
3. Accept each candidate u with probability $\hat{\lambda}_y(u)/\lambda_{\max}$.

The accepted times constitute a realisation of the IPP for that year; the procedure is repeated across all N_{year} years and mapped back to the continuous time scale.

Unlike the translation method, this approach does not condition on the observed realisation of N_y: both the event count and inter-event intervals are random under the Poisson assumption. It therefore tests temporal independence conditional on the intensity function $\hat{\lambda}_y(u)$ rather than on the observed event configuration, and is more sensitive to intensity misspecification and violations of the Poisson assumption. In practice, we use IPP simulations primarily as a diagnostic to assess the robustness of results obtained under the translation-based null model. Concordant rejections across both strategies provide stronger evidence for genuine second-order dependence beyond first-order seasonal effects.

4.2 Global envelope test

For each simulation strategy, we generate n_{sim} independent replicates of N_y under H_0 and compute the corresponding cross-K curves $\hat{K}_{xy}^{(i)}(r)$, $i = 1, \ldots, n_{\text{sim}}$. We employ the rank envelope test (Myllymäki et al., 2017), which compares the observed curve to the simulated ensemble via extreme ranks and yields an exact global p-value. The analysis is conducted on centred statistics: $\hat{K}_{xy}(r) - 2r$ for the symmetric cross-K, and $\hat{K}_{x\to y}(r) - r$ for the directional variant. The resulting global envelope $[\hat{K}^{\text{low}}(r), \hat{K}^{\text{high}}(r)]$ is assessed simultaneously over all lags r: if the observed centred curve exits the envelope at any lag, the global p-value provides evidence against H_0; otherwise H_0 is not rejected.

Observed values above the envelope indicate temporal attraction (excess co-occurrence); values below indicate inhibition (excess separation). The interpretation depends on the simulation strategy: the translation-based test is conditional on the observed realisation of N_y and its internal structure, whereas the IPP-based test conditions only on the estimated intensity $\hat{\lambda}_y(u)$, allowing one to distinguish shared first-order seasonal structure from residual second-order dependence.

5 Fire Weather Index Analysis in Three Mediterranean Regions

In this section, we investigate the behavior of the Fire Weather Index (FWI) in three fire-prone Mediterranean regions: Aquitaine, Portugal, and Catalonia, which were part of the Living Lab regions of the FIRE-RES project (https://fire-res.eu/living-labs/, last access: 18 February 2026) targeting prediction and management of extreme wildfires in Europe. Our goal is to assess how local meteorological conditions shape wildfire risk in each of these regions using a point–process framework. These regions exhibit contrasted climatic regimes while sharing recurrent exposure to severe wildfire episodes, making them well suited for a comparative event-based analysis. Due to the complex dynamic algorithmic architecture of FWI (Stocks et al., 1989), it is usually not obvious which of the underlying weather drivers have contributed most significantly to an extreme FWI event, and we use point process analysis to explore these relationships.

All variables used in this study are derived from the ERA5 reanalysis dataset (Hersbach et al., 2023), which provides spatially and temporally consistent meteorological fields at daily resolution. We have data from 2000 to 2022. The Fire Weather Index (FWI) is used as an integrated indicator of fire danger, combining information on fuel moisture, atmospheric dryness, and wind effects. The Fire Weather Index (FWI) is computed from a set of meteorological input variables. In addition to the FWI, we explicitly analyse these input variables, which are known to influence wildfire activity: near-surface air temperature, relative humidity, wind speed, global incoming shortwave radiation, precipitation, and vapour pressure deficit (VPD).

To characterise the role of antecedent hydroclimatic conditions in modulating extreme events, several studies rely on precipitation accumulation indices that explicitly account for memory effects. A classical example is the Antecedent Precipitation Index (API), originally introduced by (Kohler and Linsley, 1951) to describe a catchment's response to accumulated precipitation and natural runoff generation. The API is defined recursively on day t as a weighted sum of past precipitation, where contributions from earlier days decay exponentially, thereby assigning greater importance to recent rainfall.

More recent applications have used this concept to a broader range of environmental hazards. For instance, Jacquemin et al. (2026) used the Accumulated Precipitation Index to account for antecedent moisture conditions and long-term drying processes, explicitly highlighting its relevance for representing cumulative water availability and multi-week memory effects that cannot be captured by in-

stantaneous precipitation alone. Such indices are increasingly used in the construction and interpretation of event-based catalogues of extreme and compound events, including droughts, heatwaves, and fire-related hazards.

Our objective is not limited to assessing linear associations between FWI and its meteorological drivers. Instead, we explicitly focus on the co-occurrence structure of extreme events, adopting an event-based point process framework. This approach allows us to investigate whether extreme FWI events tend to cluster in time with extreme values of specific atmospheric variables, beyond what would be expected from their typical seasonal occurrence patterns alone.

5.1 Creation of extreme events and exploratory temporal structure

Extreme events are defined at the grid-point level in order to preserve local variability and to avoid spatial smoothing of rare and intense conditions. For each variable, empirical quantiles are computed independently at each spatial grid point using the full available temporal record over the analysis period. This pointwise approach ensures that extremes are identified relative to the local climatology rather than through spatially aggregated thresholds.

To ensure methodological consistency across variables while retaining a clear physical interpretation, extreme events are defined using upper or lower tail quantiles depending on whether high or low values are associated with enhanced fire danger. Specifically, all variables linked to increased fire risk through unusually high values are thresholded at the 99th percentile, while variables for which unusually low values are critical are thresholded at the 1st percentile.

High-end extremes (upper 99th percentile) are identified for the Fire Weather Index (FWI), near-surface air temperature, wind speed, incoming shortwave radiation and vapour pressure deficit (VPD). These conditions correspond to rare but physically meaningful situations associated with enhanced atmospheric dryness, increased energy availability, or dynamical forcing, all of which contribute to elevated fire danger or severe weather potential.

Conversely, relative humidity and the Accumulated Precipitation Index (API) are treated asymmetrically, as low values indicate dry atmospheric conditions and prolonged precipitation deficits, respectively. For these variables, extreme events are therefore defined using the lower 1st percentile, capturing situations of exceptional dryness relevant for fuel desiccation and fire spread.

Once threshold exceedances are identified at the grid-point level, extreme events are aggregated into coherent spatio-temporal structures using a connected-component analysis. Two exceedances are considered part of the same event if they occur within a spatial distance of 50 km and within a temporal window of 7 d. This aggregation step allows the identification of large-scale and persistent extreme episodes while filtering out isolated or short-lived anomalies.

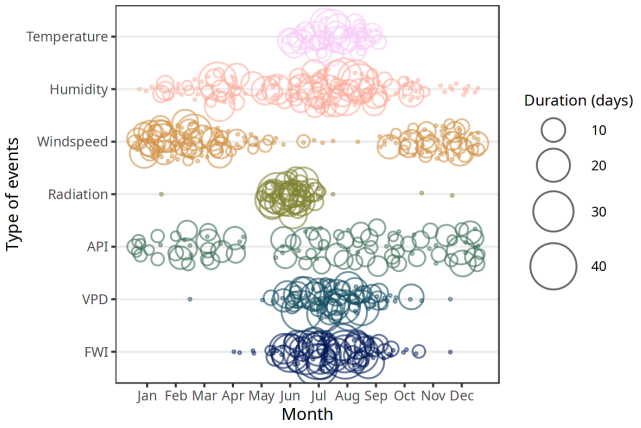


Figure 2. Multivariate timeline of extreme events in Aquitaine (2000–2022). Each symbol represents an aggregated spatio-temporal extreme event positioned by its start date. Symbol size indicates event duration.

The resulting events are characterised by their duration, spatial extent, and temporal location, and form the basis for the subsequent point-process analyses. Figure 2 presents the resulting multivariate event timeline for the Aquitaine region over the period 2000–2022, where extreme events for all variables are displayed jointly.

This representation highlights the strong seasonality shared by all variables (but not necessarily simultaneous), with most extreme events clustering between late spring and early autumn. In particular, FWI extremes are tightly concentrated during the summer months, overlapping in time with high temperature, high VPD, and low humidity events, reflecting the well-known seasonal coupling between atmospheric dryness and fire danger.

To further characterise interannual variability and to place the year 2022 within a broader climatological context, we complement the event timelines with cumulative marked point-process representations of extreme FWI events. For each year, the cumulative sum of event durations (in days) is plotted as a function of the day of year, yielding a set of annual point-process trajectories (Fig. 3).

This representation clearly shows that 2022 stands out as an exceptional year, characterised by an early onset of extreme FWI values and a markedly steeper cumulative increase during the summer period. Compared with other years, the 2022 trajectory departs from the bulk of historical variability both in terms of timing and cumulative event duration, indicating an unusually persistent and intense sequence of fire weather conditions.

Finally, Fig. 4 provides a focused view of the multivariate event timeline restricted to the year 2022. This zoomed representation makes it possible to visually assess the temporal co-occurrence and sequencing of extremes across variables during that year.

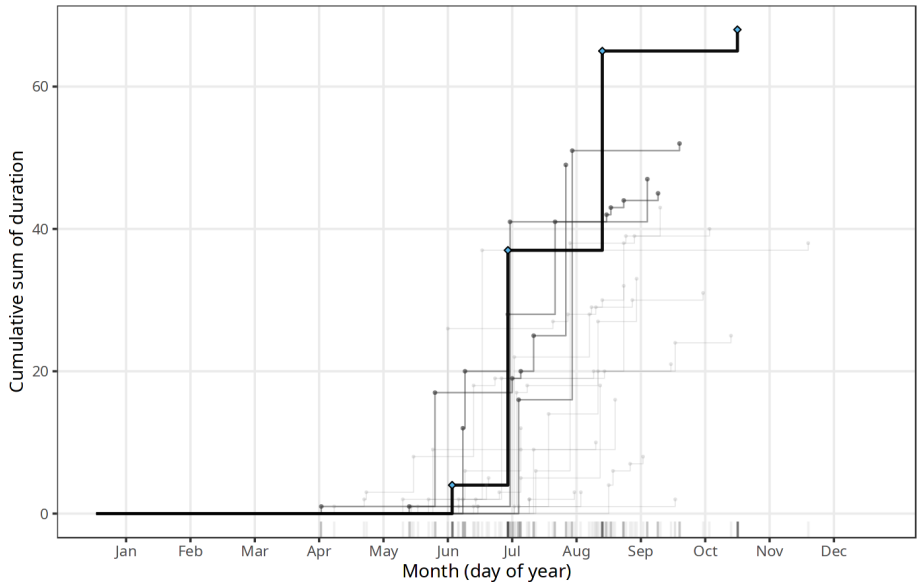


Figure 3. Cumulative marked point-process trajectories of extreme Fire Weather Index (FWI) events in Aquitaine. Each trajectory represents, for a given year, the cumulative sum of event durations (in days) as a function of the day of year. Grey trajectories correspond to individual yearly realizations (light grey: non-extreme years; dark grey: years with the highest final cumulative durations), while the year 2022 is highlighted with blue points and a black outline.

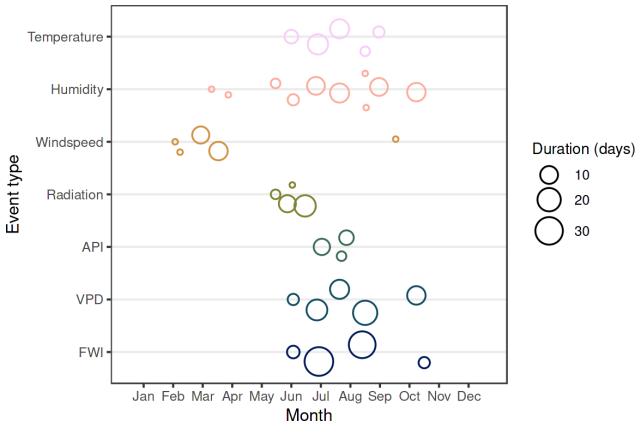


Figure 4. Multivariate timeline of extreme events in Aquitaine in 2022. Each symbol represents an aggregated spatio-temporal extreme event positioned by its start date. Symbol size indicates event duration, highlighting the persistence of several extreme episodes.

The 2022 timeline confirms the strong seasonal alignment of extremes, with clusters of long-duration FWI events occurring concurrently with extreme temperature, high VPD, and low-humidity conditions during summer. Notably, the most persistent and intense FWI episodes coincide temporally with the major wildfire outbreaks that affected southwestern France, including the large fires in the Landes forest during July and August 2022.

These exploratory visualisations provide essential motivation for adopting a point process framework, as they reveal temporal patterns and potential dependencies and motivate the subsequent use of second-order point process statistics, in particular cross-K functions, to formally assess and quantify the global and short-term temporal dependence structures between fire weather conditions and their associated meteorological drivers.

5.2 Directional Temporal Dependence Between Meteorological Drivers and FWI

To assess whether extreme meteorological conditions tend to precede episodes of extreme fire danger, we perform directional temporal dependence tests between each meteorological covariate and the Fire Weather Index (FWI). Specifically, we test the null hypothesis that events of a given covariate occur independently of subsequent FWI events within a temporal neighbourhood of radius $r = 10.5$, against alternatives corresponding to temporal attraction or inhibition.

Directional dependence is quantified using the directional cross-K function $\hat{K}_{x\to\mathrm{FWI}}(r)$, which counts only event pairs for which the covariate event occurs before the FWI event within the same annual cycle. For each covariate and region, three alternative hypotheses are considered: a two-sided alternative testing for any departure from independence, a one-sided alternative testing for temporal attraction corresponding to an excess of FWI events following the covariate, and a one-sided alternative testing for temporal inhibition corresponding to a deficit of FWI events following the covariate.

Statistical significance is assessed using the Global Envelope Test (GET), based on 999 Monte Carlo simulations un-

der two distinct null models: a inhomogeneous Poisson process conditional on the estimated seasonal intensity, and a translation-based null model that preserves the observed temporal structure of the covariate process.

Low p-values for the attraction alternative indicate that extreme covariate events tend to be followed by FWI extremes more frequently than expected under temporal independence, consistent with a short-term positive temporal association. Conversely, low p-values for the inhibition alternative indicate temporal inhibition, corresponding to a deficit of FWI events following the covariate. Non-significant two-sided p-values indicate that, when averaged over the full range of temporal lags considered, the timing of covariate events does not systematically deviate from temporal independence with respect to subsequent FWI events.

Detailed results for all regions and covariates are reported in Appendix (Tables A1, A2, and A3).

In Aquitaine, directional dependence is primarily associated with atmospheric dryness. Near-surface air temperature exhibits a strong and consistent attraction signal, with highly significant p-values under both IPP and translation simulations ($p < 0.001$). Vapour pressure deficit (VPD) also shows robust directional dependence, indicating that episodes of exceptional atmospheric dryness tend to precede extreme fire weather conditions. Relative humidity displays a significant but weaker directional signal, with low-humidity extremes occurring preferentially before FWI events. By contrast, accumulated precipitation (API) does not exhibit any significant directional dependence under either null model, suggesting that short-term precipitation deficits do not systematically precede FWI extremes. Radiation and wind speed yield non-significant results, pointing to a limited and inconsistent role as short-term precursors in this region.

Catalonia shows the strongest and most coherent directional dependence patterns among the three regions. Humidity, temperature, VPD, and wind speed all exhibit highly significant attraction effects under both IPP and translation-based null models. In particular, humidity and temperature yield extremely low p-values ($p < 0.001$), highlighting the dominant role of atmospheric dryness and heat in shaping short-term fire danger dynamics. Incoming radiation also displays significant directional dependence, indicating that high-radiation episodes tend to precede extreme FWI events more frequently than expected under independence. As in other regions, API does not show significant directional attraction, reinforcing the interpretation that precipitation-related indices primarily influence fire danger through longer-term processes.

Portugal presents a more nuanced pattern. Temperature and vapour pressure deficit again exhibit strong and consistent directional dependence, with significant attraction effects under both simulation strategies. Relative humidity also shows a clear directional signal, particularly under the translation null model, indicating that low-humidity conditions frequently precede FWI extremes. Wind speed displays only weak and model-dependent evidence of directional dependence, with significance under IPP but not under the translation model, suggesting a non-robust effect. Accumulated precipitation (API) does not show any significant directional dependence under either null model, indicating the absence of a systematic short-term temporal association with FWI extremes, despite possible longer-term relationships. Radiation remains largely independent of FWI timing in Portugal, with non-significant results under both null models.

5.2.1 Illustrative directional examples

For clarity, we do not display all directional cross-K functions in the main text. Instead, we present two representative examples from the Aquitaine region that illustrate distinct types of temporal behaviour identified by the directional Global Envelope Test. These examples also provide an illustration of our cross-K function.

Figures 5 and 6 show the directional cross-K functions testing whether extreme high temperature and low humidity events tend to precede extreme Fire Weather Index (FWI) events under the temporal translation null model, for the greater alternative.

The temperature $\rightarrow$ FWI case (Fig. 5) exhibits a clear and robust signal of temporal attraction. The observed directional cross-K curve lies systematically above the upper global envelope over a wide range of temporal lags, indicating that extreme temperature events occur more frequently than expected within several days prior to extreme FWI events. This result is consistent across simulation strategies and aligns with the well-established physical role of sustained high temperatures in driving fuel desiccation and escalating fire danger.

By contrast, the humidity $\rightarrow$ FWI case (Fig. 6) displays a weaker but still detectable signal of temporal dependence. The observed curve marginally exceeds the envelope at intermediate temporal lags, yielding a statistically significant but less pronounced departure from temporal independence. This pattern suggests that periods of unusually low humidity tend to precede extreme fire weather conditions, although with greater variability and weaker persistence than temperature-driven effects.

Together, these examples illustrate the ability of the directional cross-K framework to discriminate between strong and moderate temporal ordering relationships among meteorological variables associated with extreme fire danger. They also highlight that statistically significant dependence does not necessarily imply identical temporal structures: different covariates may exhibit distinct lead times, persistence, and strengths of association with FWI extremes.

5.2.2 Conclusion across all regions

Across all three regions, a consistent hierarchy of directional dependence emerges. Thermodynamic variables directly re-

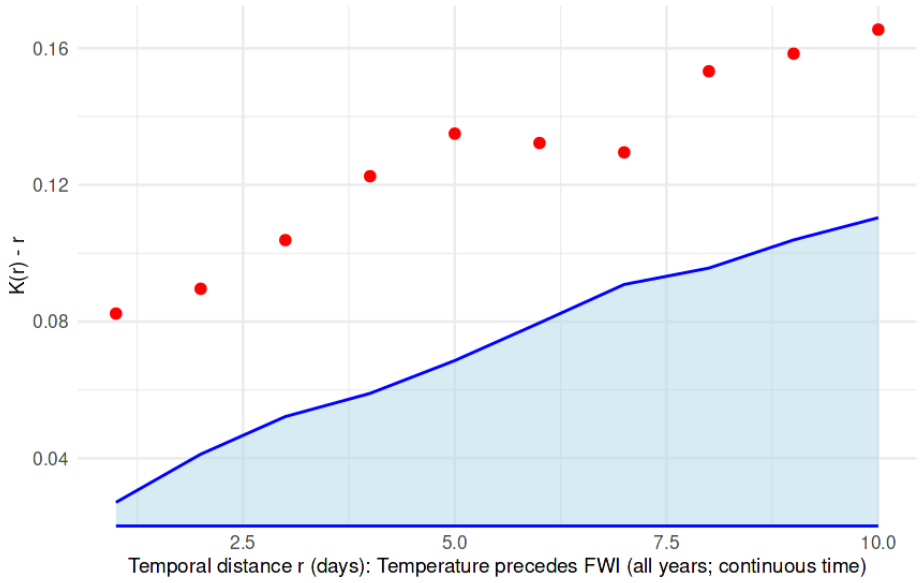


Figure 5. Directional Global Envelope Test (GET) for the temporal cross-K (more precisely $K(r)-r$) function between temperature extremes and Fire Weather Index (FWI) extremes in Aquitaine. The test assesses whether temperature extreme events systematically precede extreme fire weather conditions by considering positive temporal lags only. Dots indicate observed values of $K(r)-r$, the shaded region represents the global simulation envelope under the null hypothesis of temporal independence, and r denotes the temporal distance in days. A strong and persistent temporal attraction is observed, indicating a clear effect of temperature extremes on FWI extremes.

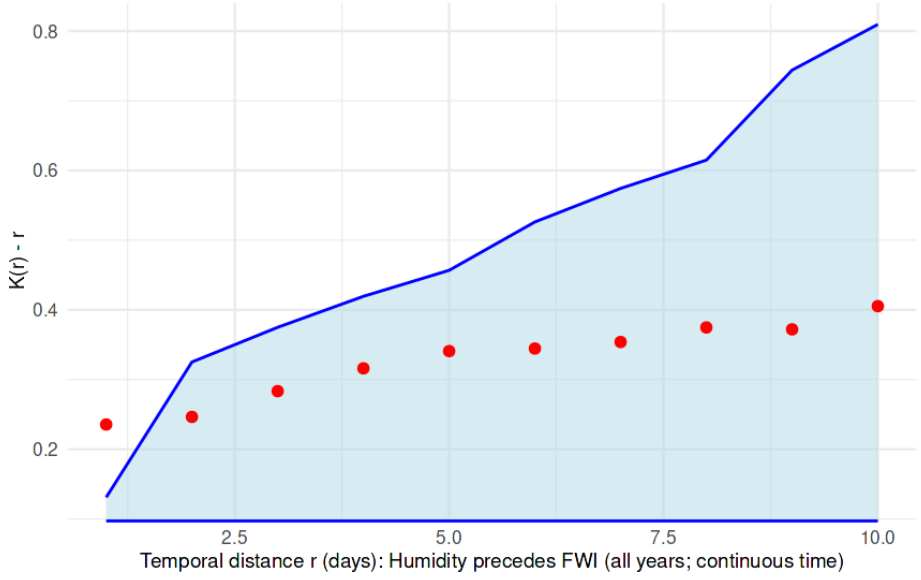


Figure 6. Directional Global Envelope Test (GET) for the temporal cross-K function between humidity extremes and Fire Weather Index (FWI) extremes in Aquitaine. Compared to Fig. 5, the temporal attraction is weaker and less persistent, indicating a more limited role of humidity extremes.

lated to atmospheric dryness and heat – temperature, vapour pressure deficit, and relative humidity – systematically precede extreme fire weather conditions, with strong agreement between IPP and translation-based null models. This concordance indicates that the detected signals are robust to the specification of the first-order temporal structure.

In contrast, accumulated precipitation does not exhibit consistent directional dependence in any region, supporting the interpretation that its influence on fire danger operates through longer-term fuel conditioning rather than short-term temporal ordering. Secondary drivers such as radiation and

wind speed show marked regional variability, with stronger directional effects in Catalonia than in Aquitaine or Portugal.

Overall, the directional GET analysis refines the global independence results by explicitly accounting for temporal ordering. It reveals that extreme fire danger is most reliably preceded by short-term atmospheric dryness and heat, while the contribution of radiative and dynamical factors varies across climatic regimes. These findings underscore the importance of region-specific mechanisms in compound fire weather dynamics.

6 Interaction between Meteorological Events in Europe

This section investigates the temporal interactions between different types of extreme meteorological events across Europe. We focus on compound and potentially interacting extremes related to convection, wind, and precipitation, and analyse their temporal co-occurrence using the point process framework presented above.

6.1 Data Sources and Study Period

The following variables were extracted to characterize extreme convective and dynamical conditions, with thresholds chosen to isolate rare and intense events:

- *Total precipitation (daily sum, in mm).* accumulated liquid and frozen water from all sources. Extremes are defined using the $q_{0.995}$ quantile of wet days only, where wet days correspond to daily precipitation exceeding 1 mm.

- *10 m wind speed (daily maximum, in m s^{-1}).* maximum horizontal wind magnitude at 10 m above the surface, computed as $\sqrt{u^2 + v^2}$ from the eastward (u) and northward (v) components. Extremes correspond to the $q_{0.995}$ quantile.

- *Convective Available Potential Energy (CAPE) (daily maximum, in J kg^{-1}).* a measure of atmospheric instability and convective potential, with extremes defined by the $q_{0.995}$ quantile.

All quantile thresholds are computed over the full study period (1941–2024), spanning more than 80 years. This choice reflects our focus on high-impact extreme events rather than on their relative rarity within specific sub-periods. By relying on long-term, stationary thresholds, we explicitly target values that are consistently associated with severe conditions and are more likely to generate substantial damage and societal impacts.

An additional motivation for this choice is that the present study does not aim to analyse temporal trends in the frequency or magnitude of extreme events. Instead, our primary interest lies in the temporal dynamics and interactions between different types of extremes, conditional on their occurrence. Using fixed quantile thresholds ensures a stable and homogeneous definition of extreme events throughout the study period, thereby avoiding confounding effects related to nonstationary thresholds and allowing a clearer interpretation of temporal dependence structures among the most extreme events.

6.2 Temporal Dependence and Choice of a Stationary Temporal Threshold

To select a stationary temporal threshold (i.e., a fixed temporal aggregation or declustering width that does not vary over time), we investigated the temporal dependence of extremes using extremograms. For each pixel time series, we defined a binary indicator I_t equal to 1 on days classified as extreme (according to the stationary quantile thresholds defined above), and 0 otherwise.

We then estimated the extremogram

$$\chi(h) = \mathbb{P}(I_{t+h} = 1 \mid I_t = 1),$$

which quantifies the conditional probability of observing an extreme event h days after a given extreme. Extremograms were computed up to $h = 30$ d for each pixel and then averaged across pixels within each region. Uncertainty bands were obtained using bootstrap resampling across pixels, while statistical significance was assessed by comparison with a null model of temporal independence.

This analysis was carried out for six combinations formed by two representative NUTS2 regions (FRL0 and FI1D) and three variables (precipitation, wind speed, and CAPE). Across all cases, extremal dependence is strongest at lag $h = 1$ and decays rapidly thereafter, becoming negligible after one to two days. Based on this consistent short-range temporal dependence structure, we retained a 2 d stationary temporal threshold for subsequent analyses. Figure 7 illustrates this behaviour for daily wind speed extremes in the FRL0 region, which provides a particularly clear example of rapid temporal decay.

6.3 Spatial Aggregation and Event Definition

Europe was partitioned using the NUTS (Nomenclature of Territorial Units for Statistics) Level 2 classification, yielding 332 regions covering the continent. These regions correspond to administrative units with typical populations between 800 000 and 3 000 000 inhabitants and characteristic spatial scales on the order of 50–150 km.

For each NUTS-2 region, ERA5 grid cells whose centroids fall within the regional boundaries were extracted, resulting in 11 796 pixel–region associations. This approach preserves sub-regional spatial variability while enabling the analysis of extreme events at a spatial scale that is relevant for climate impact assessment and policy-oriented applications. The use

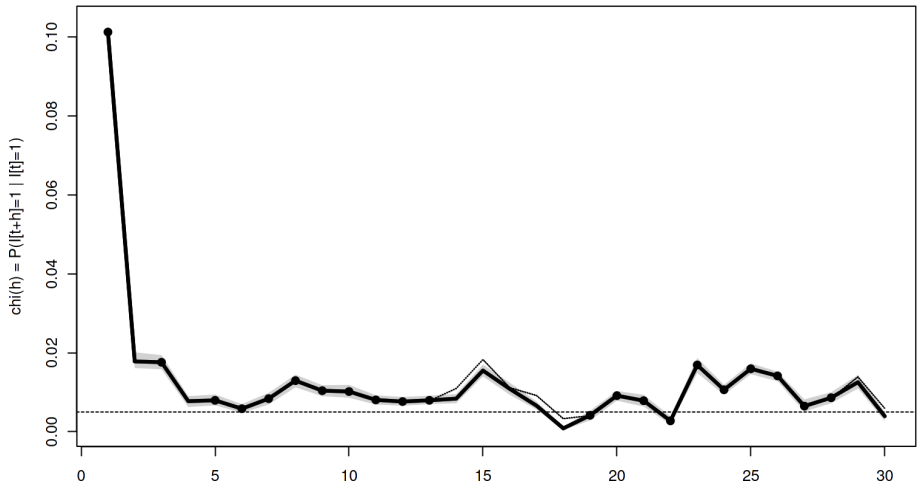


Figure 7. Regional extremogram of daily wind speed extremes in the FRL0 region. Extremes are defined by the indicator I_t, with $I_t = 1$ when wind speed exceeds the extreme threshold. The extremogram $\chi(h) = \mathbb{P}(I_{t+h} = 1 \mid I_t = 1)$ measures temporal dependence at lag h. Extremograms are computed for each grid cell and averaged over the NUTS-2 region to obtain a regional mean (solid line). The shaded area denotes the 90 % confidence interval from a spatial bootstrap resampling of grid cells while preserving temporal dependence. The dashed horizontal line corresponds to temporal independence. Dots indicate lags where the regional extremogram exceeds the upper 95 % significance bound.

of NUTS-2 regions as the spatial unit of analysis reflects our focus on regional-scale hazard interactions, where each region is considered as a distinct risk unit. Consequently, events are identified within regions to characterize how extreme conditions affect individual territories and to investigate interactions between regional risks.

Extreme events are defined through a two-step procedure. First, individual exceedances are identified at the grid-cell and daily scale whenever the variable of interest exceeds its corresponding stationary extreme threshold. Second, these exceedances are aggregated into coherent events using a spatio-temporal declustering procedure.

The declustering relies on fixed, stationary thresholds in both time and space. In the temporal dimension, exceedances separated by at most 2 consecutive days are merged into the same event. This temporal aggregation width was selected based on the analysis of binary extremograms, which consistently showed a rapid decay of short-lag extremal dependence within two days across all six region–variable combinations considered.

In the spatial dimension, exceedances occurring within a radius of 50 km are considered part of the same event. This spatial threshold reflects the characteristic spatial coherence of meteorological extremes at the ERA5 resolution and ensures that exceedances arising from the same synoptic-scale system are grouped together.

Overall, exceedances are therefore aggregated into a single event whenever they occur within both a temporal window of two days and a spatial distance of 50 km. This spatio-temporal aggregation yields individual meteorological events that may extend over multiple grid cells and several consecutive days, while avoiding artificial fragmentation due to isolated exceedances.

Consequently, events are identified within regions to characterize how extreme conditions affect individual territories and to investigate interactions between regional risks. Because declustering is performed independently within each region, a weather system propagating across several regions is represented by separate regional events rather than by a single continuously tracked event; event durations, magnitudes, and spatial extents may therefore depend on the choice of regional boundaries, which should be made carefully when applying the proposed framework to other settings.

Using a common translation-based null model ensures that differences in test outcomes across regions or variables are not driven by differences in intensity estimation or first-order temporal structure, but rather reflect genuine departures from temporal independence. This choice is particularly important in a multi-regional setting, where climatic regimes, event frequencies, and seasonal cycles vary substantially across Europe.

6.4 Same-variable temporal interaction across regions

To investigate the spatial footprint of temporal co-occurrence of extreme events across Europe, we analyse inter-regional temporal dependence using same-variable cross-K functions. Each European NUTS-2 region is compared against a single reference region, Provence–Alpes–Côte d'Azur (NUTS2_ID = FRL0), using translation-based simulations within a periodic yearly framework. The analysis tests whether extreme events occurring in a given target region

tend to occur within a short temporal window of events in the reference region more frequently than expected under temporal independence.

All tests are conducted for a temporal radius of $r = 3.5$ d and rely on a two-sided Global Envelope Test. The translation-based null model preserves the full internal temporal structure of each regional process while breaking any systematic temporal alignment between regions, thereby providing a conservative and spatially consistent reference for inference.

Spatial patterns of temporal dependence are summarised using maps of the log-transformed test statistic $-\log_{10}(p)$, which provide a continuous and interpretable measure of the strength of evidence against the null hypothesis of temporal independence. Larger values correspond to stronger departures from independence, while values close to zero indicate weak or absent evidence of temporal interaction. Compared to binary classifications based on fixed significance thresholds, these maps more clearly reveal spatial gradients and the progressive attenuation of dependence with distance from the reference region. For severe wind, shown in Fig. 8, elevated $-\log_{10}(p)$ values are observed over large parts of central and southern Europe, indicating strong and spatially coherent temporal dependence with FRL0 across wide regions. This pattern is consistent with the influence of large-scale atmospheric circulation systems that generate wind extremes over broad spatial extents. In contrast, northern Europe and parts of eastern Europe are characterised by uniformly low values, indicating a loss of temporal coherence at larger distances.

For severe precipitation, the spatial structure of dependence is more fragmented, see Fig. 9. Higher $-\log_{10}(p)$ values are primarily confined to neighbouring and intermediate-distance regions, while more distant regions exhibit values close to zero, consistent with temporal independence. This pronounced spatial attenuation highlights the more localised nature of temporal coherence for precipitation extremes compared to wind.

To assess the robustness of these patterns with respect to the choice of the reference region, the same analysis was repeated using alternative reference regions. When severe wind extremes in Upper Bavaria (DE21, Fig. 10) are used as the reference process, the resulting spatial footprint of temporal dependence appears spatially extensive. Elevated values of $-\log_{10}(p)$ are observed over large parts of Central and Northern Europe, indicating a broad-scale temporal coherence of wind extremes. Although some regional attenuation is visible with increasing distance, the dependence structure remains comparatively widespread, highlighting the capacity of wind extremes to exhibit coherent temporal behaviour over large spatial scales.

In contrast, when severe precipitation extremes in Southern Finland (FI1D, Fig. 11) are used as the reference region, the resulting spatial patterns remain strongly localised. Elevated $-\log_{10}(p)$ values are primarily confined to neighbouring or intermediate-distance regions, while more distant areas consistently exhibit values close to zero, indicating temporal independence. This confirms the limited spatial coherence of precipitation extremes, even when alternative reference regions are considered.

Taken together, these inter-regional analyses demonstrate that the spatial extent of temporal dependence depends primarily on the type of hazard considered, rather than on the specific choice of the reference region. Wind extremes exhibit broader spatial coherence, ranging from regional to continental scales depending on the reference region, whereas precipitation extremes consistently display a strongly localised dependence structure. The consistency of these patterns across multiple reference regions confirms that they reflect genuine inter-regional temporal alignment rather than region-specific artefacts. This contrast is physically consistent with the different spatial organisation of the underlying atmospheric processes. Extreme wind events are often associated with large-scale synoptic systems, such as extratropical cyclones and associated pressure gradients, which can affect large areas simultaneously. In contrast, extreme precipitation events are frequently driven by mesoscale and convective processes, whose spatial footprint is more limited and strongly influenced by local conditions such as topography and moisture availability.

From an applied perspective, such dependence structures are highly relevant for the assessment of spatially compounding events. Regions exhibiting strong temporal dependence with a given reference region are more likely to experience concurrent or closely timed extreme events, increasing the potential for spatially aggregated impacts. Conversely, regions showing systematic temporal independence may provide more robust opportunities for risk spreading and mitigation in the context of spatially distributed hazard exposure.

6.5 Cross-variable temporal interaction within regions

To investigate the temporal interaction between different types of extreme events within individual regions, we conducted intra-regional analyses using cross-type K-functions. In contrast to the inter-regional setting, where events in different regions are compared, this analysis focuses on interactions between event types occurring within the same NUTS-2 region. The same translation-based simulation framework and periodic yearly structure as in the inter-regional analyses are employed, ensuring full methodological consistency across scales.

All tests are performed using a short temporal interaction radius of $r = 3.5$ d and rely on a two-sided Global Envelope Test. As before, translation-based simulations preserve the complete seasonal and temporal structure of each regional process while breaking any systematic temporal alignment between event types. Results are summarised using maps of the log-transformed test statistic $-\log_{10}(p)$, providing a con-

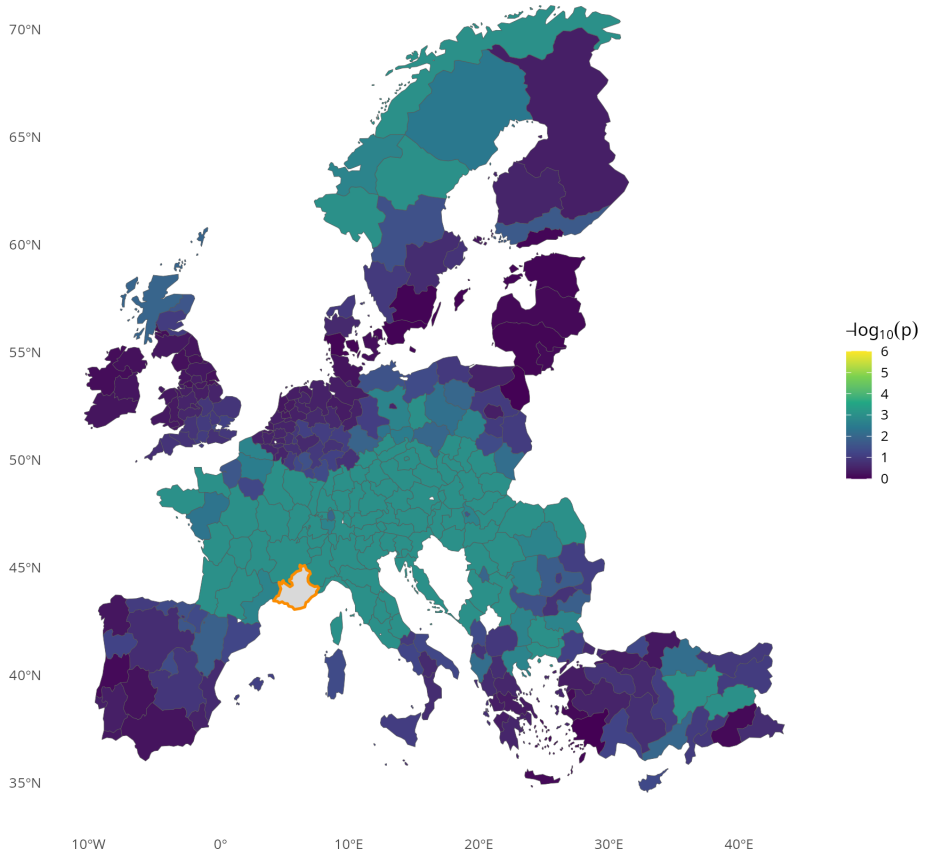


Figure 8. Spatial distribution of the $-\log_{10}(p)$ values from the inter-event temporal dependence test between severe wind extremes and FRL0 across Europe. Higher values indicate stronger evidence of temporal dependence. Results are shown for distances up to the maximum interaction range considered, with p-values floored at 10^{-6} and the color scale capped at 6.

tinuous measure of the strength of evidence against the null hypothesis of temporal independence.

6.5.1 Severe precipitation vs. severe wind

The strongest and most spatially coherent intra-regional temporal dependence is observed between severe precipitation and severe wind extremes. Across a large majority of NUTS-2 regions in Europe, the null hypothesis of temporal independence is rejected, resulting in an almost continuous continental pattern of dependence. This widespread intra-regional dependence is clearly visible in the spatial distribution of the $-\log_{10}(p)$ values (Fig. 12), which reveals an almost continuous pattern of temporal coupling between severe wind and severe precipitation extremes across Europe.

Overall, the dependence structure appears largely symmetric when considering undirected interactions, indicating that extreme precipitation and extreme wind events tend to occur in close temporal proximity within regions. However, directional analyses yield highly similar results, suggesting that the observed co-occurrence is not dominated by a single systematic temporal ordering but rather reflects tightly coupled meteorological processes acting on short time scales.

Despite this broad coherence, several regional specificities emerge. In particular, Mediterranean regions and parts of Great Britain exhibit distinct patterns, with either enhanced or reduced temporal dependence compared to the continental background. A small number of regions, often peripheral or characterised by limited event counts, show weak or absent dependence, which may partly reflect reduced statistical power rather than fundamentally different temporal dynamics.

6.5.2 CAPE preceding severe wind

We next investigate directional intra-regional temporal interactions between convective instability and wind extremes by analysing the cross-type temporal interaction from CAPE to severe wind within each NUTS-2 region. The directional test is performed using the greater alternative, assessing whether CAPE extremes tend to precede severe wind events more frequently than expected under temporal independence (Fig. 13).

The resulting spatial pattern indicates that, across most European regions, the evidence for directional temporal dependence from CAPE to severe wind is weak or absent, suggest-

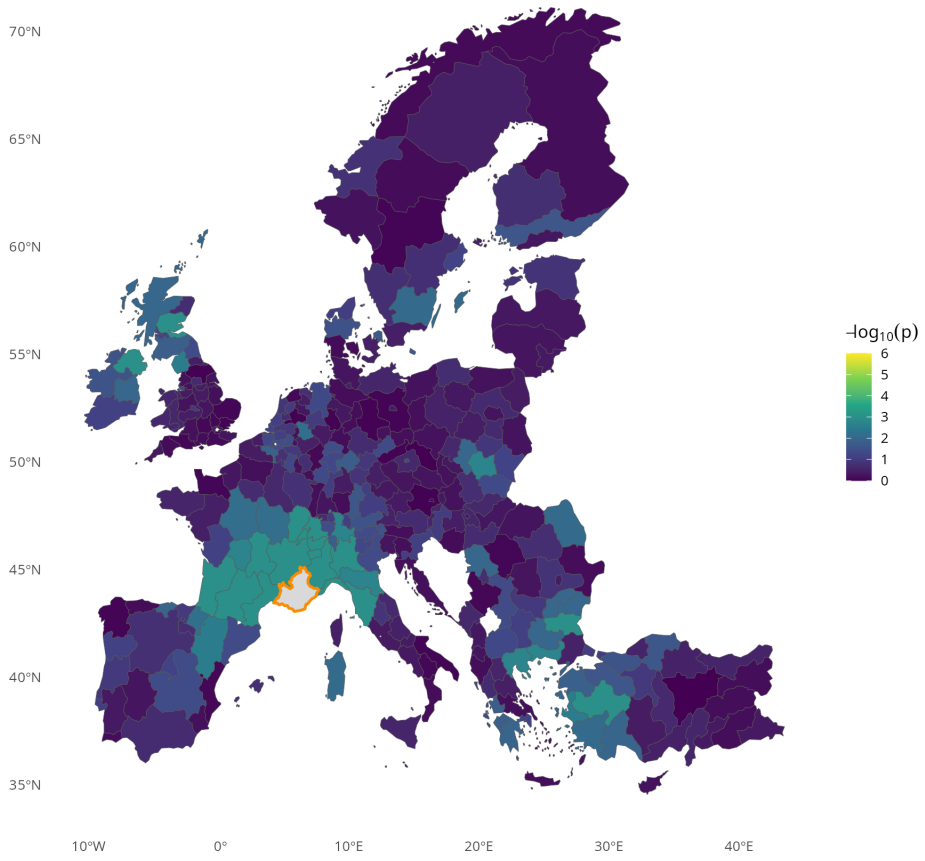


Figure 9. Spatial distribution of the $-\log_{10}(p)$ values from the inter-event temporal dependence test between severe precipitation extremes and FRL0 across Europe. Higher values indicate stronger evidence of temporal dependence. Results are shown for distances up to the maximum interaction range considered, with p-values floored at 10^{-6} and capped at 6.

ing limited systematic behaviour at the intra-regional scale. However, notable regional exceptions emerge. In particular, parts of Scandinavia and Great Britain exhibit elevated $-\log_{10}(p)$ values, indicating statistically significant temporal clustering of severe wind events following CAPE extremes.

In addition, several regions located within or in close proximity to major European mountain ranges, including the Alpine arc, the Pyrenees, and parts of the Balkan region, also display enhanced levels of statistical significance. Although this observation has not been formally tested statistically, such spatial coherence may suggest that regional geographical or climatological factors could modulate the strength of the temporal association between CAPE and severe wind extremes. In these areas, CAPE extremes may therefore appear to act more frequently around severe wind events than would be expected under temporal independence. Overall, the results suggest that the temporal relationship between CAPE and severe wind is only evident in specific regional contexts, rather than uniformly across Europe, and that this dependence likely reflects broader regional characteristics rather than convective instability alone.

6.5.3 CAPE preceding severe precipitation

We then examine directional intra-regional temporal interactions from CAPE to severe precipitation extremes, again focusing on the greater alternative to test whether CAPE events systematically precede precipitation extremes within regions (Fig. 14).

In contrast to the CAPE-wind case, the spatial pattern for CAPE preceding severe precipitation reveals widespread and robust temporal dependence across much of Europe. Elevated $-\log_{10}(p)$ values are observed in a large majority of NUTS-2 regions, indicating frequent temporal clustering of precipitation extremes shortly after CAPE extremes. This result is consistent with the fundamental role of convective instability in the initiation of intense precipitation events.

Nevertheless, several regions deviate from this general behaviour. In particular, Mediterranean regions exhibit weaker or absent directional dependence from CAPE to severe precipitation. This result is consistent with the previously identified weaker temporal coupling between severe wind and severe precipitation in these areas, suggesting that precipitation extremes there are less systematically associated with convective instability. More generally, these regional differ-

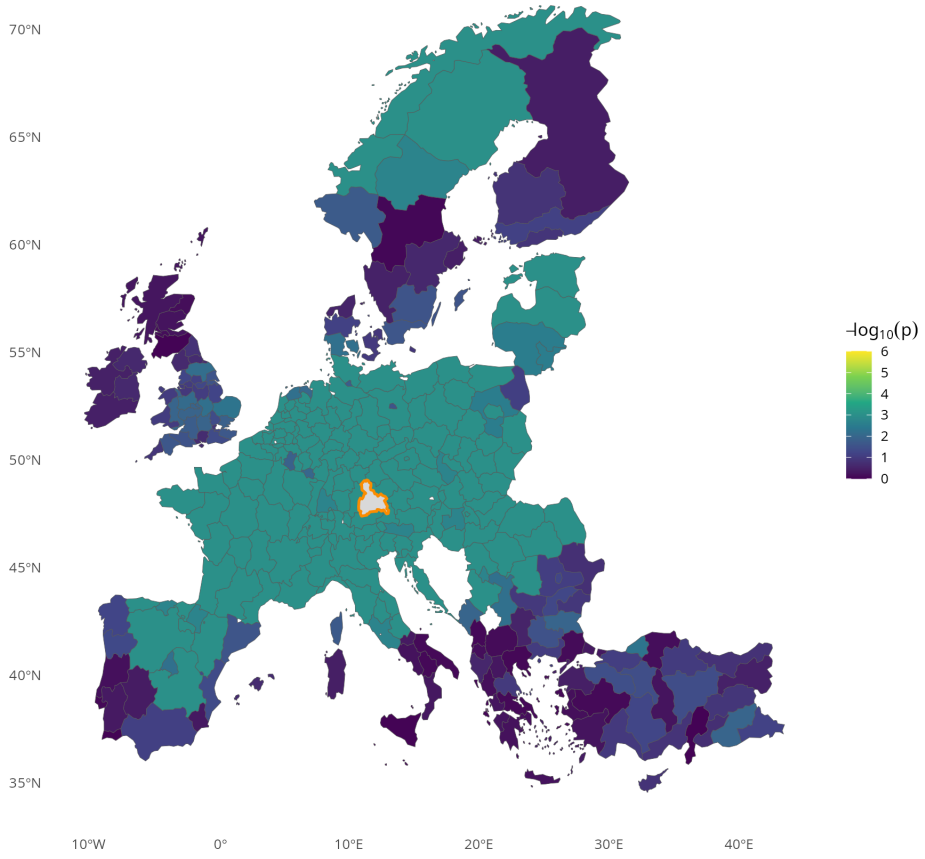


Figure 10. Spatial distribution of the $-\log_{10}(p)$ values from the inter-event temporal dependence test between severe wind extremes and the reference region DE21 (Upper Bavaria). Elevated values extend over a large part of Europe, indicating a broad-scale temporal coherence of wind extremes.

ences indicate that the strength of the CAPE–precipitation relationship varies across Europe, likely reflecting the coexistence of distinct precipitation-generating regimes rather than a uniform convective control. In Mediterranean regions, extreme precipitation can also be driven by mechanisms that are only partially captured by atmospheric instability, including moisture-rich synoptic systems, Mediterranean cyclogenesis, and orographic lifting, which may explain the weaker dependence with CAPE compared with more continental convective regimes.

Taken together, these intra-regional analyses demonstrate the usefulness of cross-variable temporal interaction tests for identifying temporal compounding events within regions. By explicitly quantifying short-term temporal clustering between different types of extremes, this framework allows the detection of potential cascading event sequences, where the occurrence of one extreme increases the likelihood of another within a limited time window. The strong wind–precipitation coupling identified across central and northern Europe is physically consistent with the passage of extratropical cyclones, whose organised structure simultaneously produces both intense surface winds and heavy precipitation over affected regions. In contrast, the comparatively weak and spatially heterogeneous CAPE–precipitation coupling suggests that convective instability does not systematically translate into coherent precipitation extremes at the daily timescale and regional spatial scale considered here, possibly reflecting the sub-daily and highly localised nature of convective precipitation events that are not fully captured by ERA5 at its resolution. The characteristic timescale over which coupling is detected – as revealed by the lag structure of the cross-K function – can directly inform the choice of accumulation periods in catastrophe models and the design of multi-hazard alert thresholds in operational early-warning systems. The results highlight that such cascading behaviour is strongly variable across event types and regions, underscoring the importance of accounting for intra-regional temporal dependencies when assessing compound risk and the potential for successive or overlapping impacts.

We also verified the robustness of these conclusions through sensitivity analyses on the extreme threshold, the declustering parameters, and the temporal interaction radius, which yielded consistent results across all tested configurations.

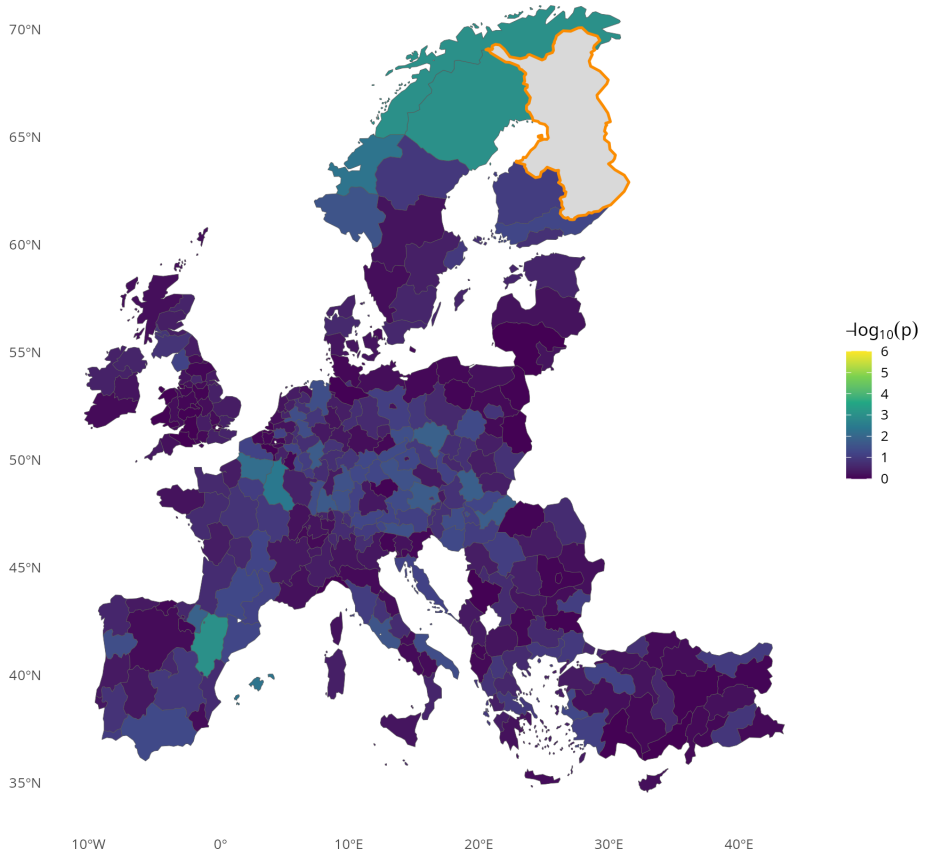


Figure 11. Spatial distribution of the $-\log_{10}(p)$ values from the inter-event temporal dependence test between severe precipitation extremes and the reference region FI1D (Southern Finland). The spatial footprint of temporal dependence is highly localised, confirming the limited spatial coherence of precipitation extremes compared to wind.

7 Discussion and Conclusion

This study demonstrates the usefulness of point process methods, and in particular cross-type K-functions combined with Global Envelope Tests, for analysing temporal dependencies between extreme weather events. By adopting an event-based perspective, the proposed framework moves beyond traditional correlation-based approaches applied to continuous variables and directly addresses questions of temporal clustering, co-occurrence, and sequencing that are central to the assessment of compound and cascading risks.

Applied to extreme precipitation, severe wind, and atmospheric instability (CAPE) across European NUTS-2 regions, the analyses reveal a clear hierarchy of temporal dependence structures. Inter-regional results obtained using the translation simulation method indicate that certain hazards, such as severe wind, tend to exhibit comparatively broad spatial coherence in their temporal alignment across regions. In contrast, extreme precipitation displays a more fragmented and spatially localised pattern of temporal dependence, suggesting a stronger sensitivity to regional-scale processes.

At the intra-regional scale, the framework highlights pronounced temporal coupling between severe precipitation and severe wind across large parts of Europe, indicating frequent short-term co-occurrence of these hazards within regions. In contrast, cross-variable interactions involving CAPE appear substantially weaker and more spatially heterogeneous. Directional analyses further suggest that CAPE precedes severe wind only in specific subsets of regions, notably including areas located within or in close proximity to major mountain ranges, while many regions exhibit little or no systematic ordering behaviour.

The spatial concentration of CAPE–wind dependence in mountainous regions is particularly noteworthy. While the present analysis remains purely statistical, this pattern appears plausible in light of recent synthesis work on severe convection in complex terrain, which emphasises the role of orography in modulating convective initiation and storm intensification (Fischer et al., 2025). In these regions, the mechanical lifting of air masses by terrain features and associated thermodynamic destabilisation are known to favour the rapid development of convective systems, which in turn generate both elevated CAPE and severe surface winds in close temporal succession. The fact that our framework independently detects a corresponding regional signal suggests that

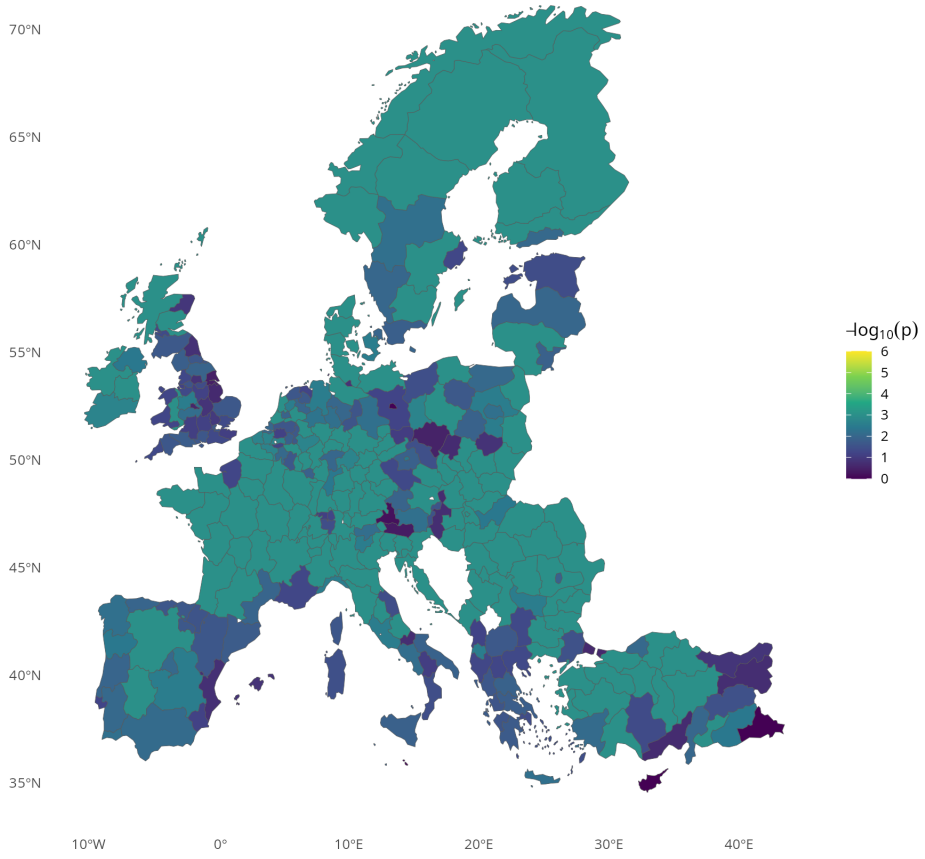


Figure 12. Spatial distribution of the $-\log_{10}(p)$ values from the intra-regional temporal dependence test between severe wind and severe precipitation extremes across European NUTS-2 regions. The analysis is conducted within each region using the same translation-based simulation framework and temporal interaction radius ($r = 3.5$ d) as in the inter-regional setting. Higher values indicate stronger evidence of temporal dependence between the two hazard types within regions, while values close to zero indicate weak or absent dependence.

the identified dependence structure is unlikely to be purely artefactual and may reflect meaningful differences in event-generating regimes across Europe. By contrast, the absence of systematic CAPE–wind sequencing in maritime regions such as Great Britain and parts of the Mediterranean basin is consistent with the predominance of synoptic-scale wind events driven by extratropical cyclones rather than convective activity, for which CAPE is not expected to precede.

These physical contrasts carry direct implications for compound risk assessment. In regions where CAPE is detected as a temporal precedence to severe wind – notably those in or near major mountain ranges – elevated convective instability could serve as an early-warning indicator, allowing civil protection authorities to anticipate a heightened probability of imminent wind damage following periods of atmospheric destabilisation. Conversely, in regions where no such ordering relationship is identified, such as maritime and Mediterranean areas, CAPE monitoring provides little added value for short-term wind risk anticipation, and early-warning strategies must rely on synoptic-scale dynamical indicators instead. Similarly, the strong temporal coupling detected between severe wind and extreme precipitation across large parts of central and northern Europe implies that regions exposed to both hazards face a non-negligible probability of concurrent stress, which should be explicitly accounted for in regional multi-hazard risk models. More broadly, the framework is not restricted to the hazard triplet considered here: it could equally be applied to other combinations of meteorological or environmental variables wherever the temporal sequencing of discrete extreme events is of practical concern for risk assessment or early-warning system design.

These results emphasise that physically related variables do not necessarily translate into consistent temporal clustering when analysed through discrete extreme events and short interaction windows. The observed heterogeneity across regions and hazard pairs points to the coexistence of distinct regional regimes rather than a uniform dependence structure. In particular, several regions within the Mediterranean basin and across Great Britain exhibit comparatively weak temporal dependence between severe wind and extreme precipitation, a feature that is also reflected in reduced dependence between CAPE and extreme precipitation in these same regions. This internal consistency further supports the interpretation of region-specific compound-event behaviour.

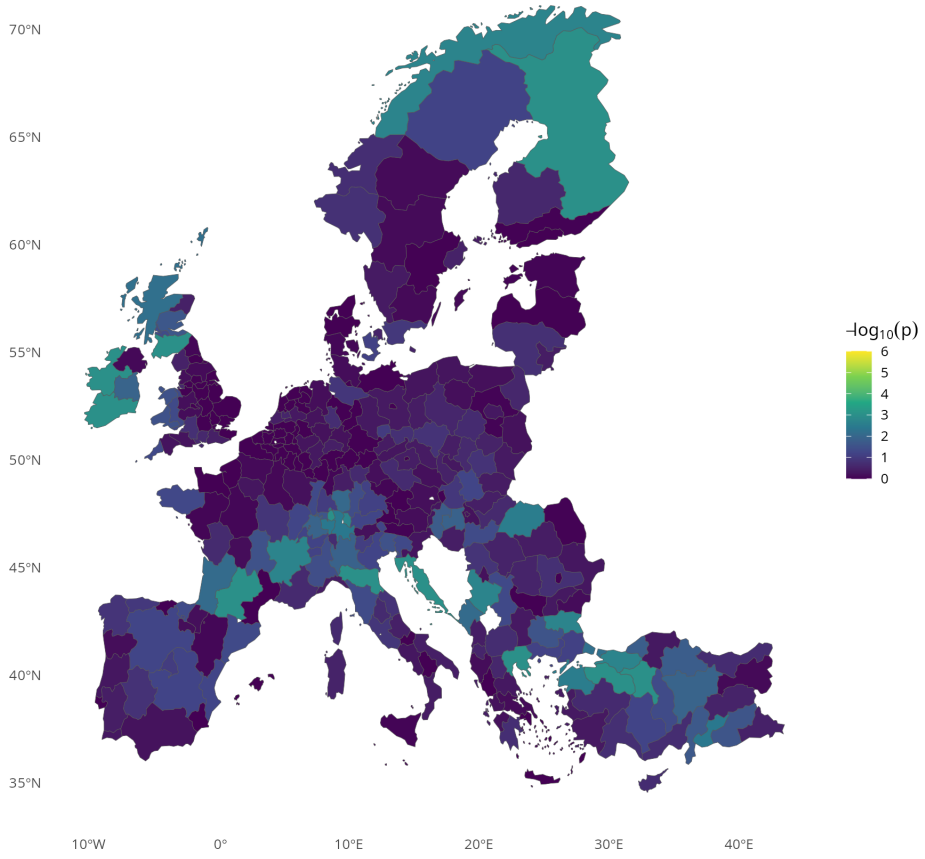


Figure 13. Spatial distribution of the $-\log_{10}(p)$ values from the directional intra-regional temporal dependence test between CAPE extremes and severe wind extremes across European NUTS-2 regions. The test is performed in the direction CAPE → severe wind using the greater alternative. Higher values indicate stronger evidence of temporal clustering of severe wind events following CAPE extremes.

Beyond meteorological interpretation, a key contribution of this work lies in its methodological and applied relevance. By explicitly quantifying short-term temporal dependence between different event types, the proposed framework provides a principled way to identify temporally compounding events and potential cascading sequences within regions, as well as coordinated or near-synchronous extremes across regions. Such information is directly relevant for risk assessment, emergency planning, and the analysis of spatially compounding hazards, as regions exhibiting strong temporal dependence are more likely to experience overlapping or successive impacts within limited time windows. Crucially, the framework moves beyond stating which hazard pairs co-occur and provides a quantitative characterisation of the interaction timescale. The shape of the estimated cross-K function, and in particular the lag at which it departs most strongly from the simulation envelopes, gives an indication of the typical temporal separation between events and can therefore inform the design of risk accumulation periods in catastrophe models or the time windows used in multi-hazard impact assessments.

Several avenues for future development emerge from this work. Methodologically, extending the framework to marked point processes would allow the joint analysis of event timing and intensity or impact. Further extensions to fully spatio-temporal K-functions could enable the simultaneous assessment of spatial and temporal interaction structures. From an applied perspective, incorporating large-scale climate indices or circulation-based classifications – such as weather regime assignments – could help contextualise and explain the detected dependence patterns without imposing causal assumptions, and could clarify whether the identified regional heterogeneity reflects stable structural differences in event-generating mechanisms or variability driven by circulation modes.

The use of ERA5 reanalysis provides a spatially and temporally consistent basis for continental-scale analyses, but several limitations should be acknowledged. As a reanalysis product, ERA5 inevitably reflects model-related uncertainties, which are particularly relevant for convective variables such as CAPE. Moreover, the daily time step combined with a spatial resolution of 0.25° limits the ability to capture short-lived and highly localised interactions, as individual

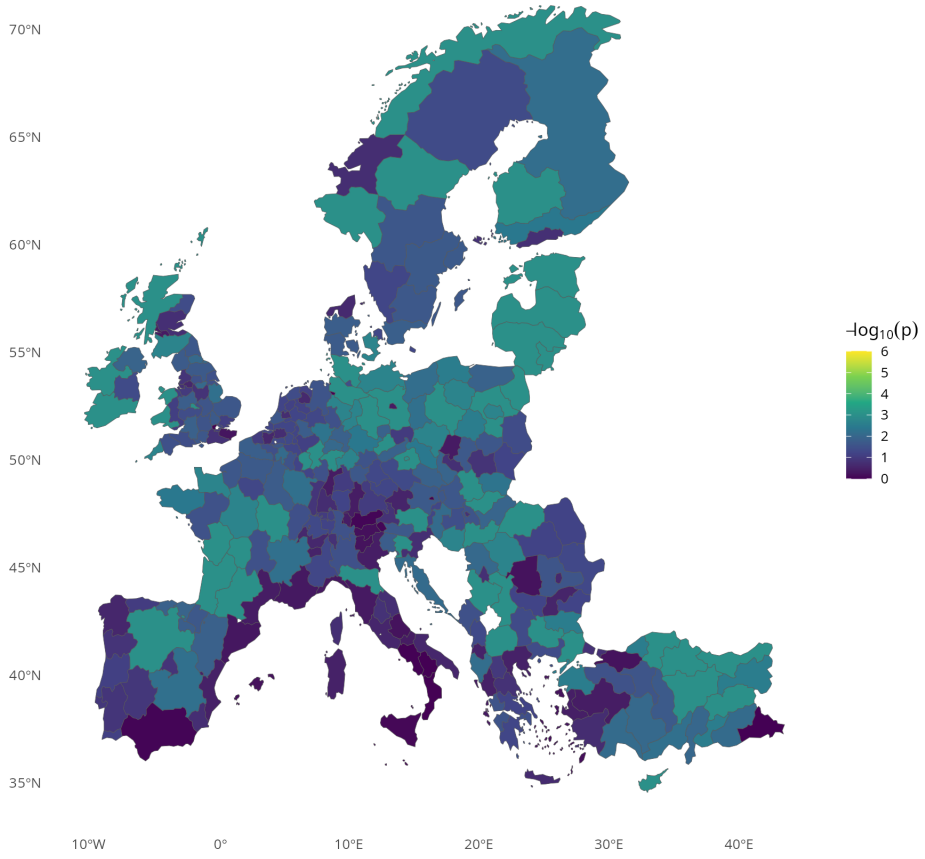


Figure 14. Spatial distribution of the $-\log_{10}(p)$ values from the directional intra-regional temporal dependence test between CAPE extremes and severe precipitation extremes across European NUTS-2 regions. The test is performed in the direction CAPE → severe precipitation using the greater alternative. Higher values indicate stronger evidence of temporal clustering of precipitation extremes following CAPE extremes.

convective cells and associated extremes are not explicitly resolved. The identification of extreme events further depends on methodological choices regarding thresholds and clustering parameters, which influence the resulting point processes and should be interpreted as representations of coherent extreme episodes rather than exact physical reconstructions.

Recent efforts to construct event-based catalogues of extreme and compound climate events further motivate the relevance of this approach. Initiatives such as the global compound-event database of Weynants et al. (2025) and the ClimaMeter framework (Faranda et al., 2024; Faranda, 2025) provide structured collections of discrete events characterised by their timing, location, and attributes. The point process framework developed here is well suited to the analysis of such catalogues, offering a consistent statistical approach to quantify clustering and cross-dependence across temporal and spatial scales.

Finally, integrating socio-economic impact data represents a key challenge and opportunity for future research. Linking meteorologically defined compound events to observed impacts would allow direct assessment of whether temporal clustering translates into compounded losses or disruptions, and would provide an empirical basis for validating the risk implications inferred from dependence patterns alone. While impact datasets remain heterogeneous and incomplete, the combination of reanalysis-based event detection with point process methods provides a robust foundation for advancing compound-risk analysis.

In conclusion, point process approaches offer a flexible and interpretable framework for analysing temporal dependencies between extreme events. By focusing on the timing and clustering of discrete events, they complement existing methods based on continuous variables and provide insights that are directly relevant for understanding compound and cascading hazards across regions and event types. The identification of region-specific dependence structures, and in particular the detection of asymmetric temporal relationships that may reflect physical cascading mechanisms, opens concrete directions for improving multi-hazard early-warning systems and for building more realistic compound-risk assessments in operational and planning contexts.

Appendix A: Tables of *p*-values

Table A1. Directional covariate → FWI GET *p*-values for Aquitaine. GET: global envelope test; IPP: inhomogeneous Poisson process; Translation: translation test; API: antecedent precipitation index; VPD: vapour pressure deficit. Significant *p*-values (< 0.05) are shown in bold.

	IPP			Translation		
Covariate	Less	Two-sided	Greater	Less	Two-sided	Greater
Temperature	1.000	**0.001**	**0.001**	1.000	**0.001**	**0.001**
Humidity	0.991	**0.040**	**0.015**	0.986	0.055	**0.034**
Wind speed	0.772	0.322	0.117	0.784	0.350	0.136
Radiation	0.992	0.094	0.063	0.986	0.159	0.058
API	0.794	0.505	0.271	0.843	0.605	0.279
VPD	1.000	**0.012**	**0.003**	0.999	**0.003**	**0.002**

Table A2. Directional covariate → FWI GET *p*-values for Catalonia. Abbreviations as in Table A1. Significant *p*-values (< 0.05) are shown in bold.

	IPP			Translation		
Covariate	Less	Two-sided	Greater	Less	Two-sided	Greater
Temperature	1.000	**0.001**	**0.001**	1.000	**0.001**	**0.001**
Humidity	1.000	**0.002**	**0.001**	1.000	**0.003**	**0.004**
Wind speed	0.874	**0.004**	**0.003**	0.898	**0.009**	**0.006**
Radiation	0.973	**0.045**	**0.024**	0.953	0.127	**0.033**
API	0.427	0.802	0.494	0.441	0.673	0.487
VPD	1.000	**0.001**	**0.001**	1.000	**0.004**	**0.002**

Table A3. Directional covariate → FWI GET *p*-values for Portugal. Abbreviations as in Table A1. Significant *p*-values (< 0.05) are shown in bold.

	IPP			Translation		
Covariate	Less	Two-sided	Greater	Less	Two-sided	Greater
Temperature	1.000	0.080	**0.001**	1.000	**0.001**	**0.002**
Humidity	0.997	0.065	**0.024**	0.993	0.082	**0.030**
Wind speed	0.813	0.119	**0.048**	0.814	0.116	0.059
Radiation	0.988	0.196	0.090	0.989	0.173	0.084
API	0.942	0.318	0.131	0.926	0.400	0.175
VPD	1.000	**0.001**	**0.001**	0.996	**0.003**	**0.002**

Appendix B: Pseudo-code algorithms

Algorithm B1 Overall workflow for compound-event analysis using point processes.

Inputs: ERA5 daily gridded fields for variables $v \in \mathcal{V}$; NUTS regional partition (e.g. NUTS-2) with regions $g \in \mathcal{G}$; quantile specification (p_v, tail_v); connectivity thresholds $(\delta_{\text{space}}, \delta_{\text{time}})$; set of radii $\mathcal{R}$ at which the $K(r)$ functions are evaluated (in days); simulation budget n_{sim}; null method (translation or IPP).
Outputs: Regional event catalogues; point processes over the full observation period (with DOY coordinate $u \in [0, 1)$); seasonal intensities $\hat{\lambda}(u)$; observed and simulated K curves; Global Envelope Test (GET) p-values; maps and figures.

(A) Construct spatio-temporally clustered extreme-event catalogues per NUTS region (Algorithm B2)
(B) Convert event onsets to point-process times with DOY coordinate $u \in [0, 1)$ and continuous time t in days (Algorithm B3)
(C) Estimate seasonal intensities $\hat{\lambda}(u)$ via periodic KDE (Algorithm B4)
(D) Compute observed cross-K curves (and optionally directional cross-K) for radii $r \in \mathcal{R}$ (Algorithm B5)
(E) Simulate under translation or IPP, build global envelopes on centred curves, and compute GET p-values (Algorithm B6)
(F) Aggregate results (tables) and produce maps (binary, $-\log_{10} p$, and extremeness proxy)

Algorithm B2 Construction of spatio-temporal extreme-event catalogues by NUTS region.

Inputs: Daily fields $X^{(v)}_{\ell,t}$; NUTS regions g; quantile (p_v, tail_v) (typically lower tail for API, humidity); δ_{space}, δ_{time}.
Outputs: Event list $\mathcal{E}^{(v)}_g$ by region and variable.

for $g \in \mathcal{G}$ **do**
  for $v \in \mathcal{V}$ **do**
    ♯ *Local thresholds.*
    for $\ell \in g$ **do**
      $\tau^{(v)}_\ell \leftarrow \text{quantile}_{p_v}(\{X^{(v)}_{\ell,t}\}_t)$
    end for
    ♯ *Exceedance set and marks (lower tail by default).*
    $\mathcal{P}^{(v)}_g \leftarrow \varnothing$
    for $\ell \in g,\ t$ **do**
      if $X^{(v)}_{\ell,t}$ is extreme relative to $\tau^{(v)}_\ell$ **then**
        $\mathcal{P}^{(v)}_g \leftarrow \mathcal{P}^{(v)}_g \cup \{(\ell, t)\}$
        $m^{(v)}_{\ell,t} \leftarrow \begin{cases} \tau^{(v)}_\ell - X^{(v)}_{\ell,t}, & \text{lower tail} \\ X^{(v)}_{\ell,t} - \tau^{(v)}_\ell, & \text{upper tail} \end{cases}$
      end if
    end for
    ♯ *Connectivity graph on exceedances.*
    Build $G^{(v)}_g = (\mathcal{P}^{(v)}_g, \mathcal{A})$ with edges if $d_{\text{space}} \le \delta_{\text{space}}$ and $|t_1 - t_2| \le \delta_{\text{time}}$.
    ♯ *Events = connected components of the graph.*
    for connected components C of $G^{(v)}_g$ **do**
      $t^{\text{start}}_C \leftarrow \min t,\ t^{\text{end}}_C \leftarrow \max t,\ \Delta t_C \leftarrow t^{\text{end}}_C - t^{\text{start}}_C + 1$
      $M_C \leftarrow \sum_{(\ell,t)\in C} m^{(v)}_{\ell,t}$
      Store $(t^{\text{start}}_C, t^{\text{end}}_C, \Delta t_C, M_C)$ in $\mathcal{E}^{(v)}_g$
    end for
  end for
end for

Algorithm B3 Creation of point-process times over the full observation period.

Inputs: Event catalogues $\mathcal{E}_g^{(v)}$ with onset dates t^{start}, for each NUTS region $g \in \mathcal{G}$.
Outputs: For each region g and variable v: event times t (days over full record), and annual-cycle coordinates $u \in [0, 1)$.

for $g \in \mathcal{G}$ **do**
  for $v \in \mathcal{V}$ **do**
    for events $e \in \mathcal{E}_g^{(v)}$ **do**
      ♯ *Year index from onset date.*
      Extract calendar year index $y(e) \in \{1, \ldots, N_{\text{year}}\}$ from t_e^{start}
      ♯ *Day-of-year and annual-cycle coordinate.*
      Compute day-of-year $\text{DOY}(e) \leftarrow \text{doy}(t_e^{\text{start}})$
      $u(e) \leftarrow (\text{DOY}(e) - 1)/T \in [0, 1)$
      ♯ *Continuous time in days over the full record.*
      $t(e) \leftarrow (y(e) - 1)\,T + \text{DOY}(e)$
      Store $(t(e), u(e))$ as an event of the process $N_g^{(v)}$
    end for
  end for
end for

Algorithm B4 Seasonal intensity estimation on the annual cycle (periodic KDE).

Inputs: Annual times $\{u_i\}_{i=1}^n \subset [0, 1)$ pooled across years; bandwidth h; kernel K (Gaussian).
Outputs: Seasonal intensity estimate $\hat{\lambda}(u)$ on $[0, 1)$ (events per year).

♯ *Pool annual-cycle coordinates across years.*
Pool all annual times across years: $\{u_i\}_{i=1}^n$.
♯ *Periodic (circular) KDE on* $[0, 1)$.
$\hat{f}(u) \leftarrow \dfrac{1}{nh} \sum_{i=1}^{n} \sum_{k \in \{-1,0,1\}} K\left(\dfrac{u - (u_i + k)}{h}\right)$.
♯ *Convert density to seasonal intensity (events per year).*
$\hat{\lambda}(u) \leftarrow n_{\text{year}}\, \hat{f}(u)$, where $n_{\text{year}} = n/N_{\text{year}}$ is the mean number of events per year.
♯ *Working on* $u \in [0, 1)$ *enforces periodicity.*

Algorithm B5 Observed cross-K and directional cross-K over the full observation period.

Inputs: For a given NUTS region g: event pairs $(t_i, u_i) \in N_{x,g}$ and $(s_j, u_j) \in N_{y,g}$; seasonal intensities $\hat{\lambda}_x, \hat{\lambda}_y$ on $[0, 1)$; set of radii $\mathcal{R}$ (days); year length T; number of years N_{year}.
Outputs: Observed curves $\hat{K}_{xy}^{\text{obs}}(r)$ (and optionally $\hat{K}_{x \to y}^{\text{obs}}(r)$) for $r \in \mathcal{R}$.

♯ *Total observation length.*
Define $T_{\text{tot}} \leftarrow N_{\text{year}}\, T$.
♯ *Time distance (choose periodic version if desired).*
Define $d(t, s) \leftarrow |t - s|$ (or $d(t, s) \leftarrow \min\{|t - s|,\ T_{\text{tot}} - |t - s|\}$ if periodic).
for $r \in \mathcal{R}$ **do**
  $\hat{K}_{xy}^{\text{obs}}(r) \leftarrow 0$
  for $(t_i, u_i) \in N_{x,g}$ **do**
    for $(s_j, u_j) \in N_{y,g}$ **do**
      $\hat{K}_{xy}^{\text{obs}}(r) \mathrel{+}= \dfrac{\mathbf{1}\big(d(t_i, s_j) \le r\big)}{\hat{\lambda}_x(u_i)\,\hat{\lambda}_y(u_j)}$
    end for
  end for
  $\hat{K}_{xy}^{\text{obs}}(r) \leftarrow \hat{K}_{xy}^{\text{obs}}(r)/T_{\text{tot}}$
end for
♯ *Directional version.*
Replace $\mathbf{1}(d \le r)$ by $\mathbf{1}\big(0 \le (s_j - t_i) \le r\big)$ (or $(s_j - t_i) \bmod T_{\text{tot}}$ if periodic).

Algorithm B6 Translation-based null model and Global Envelope Test (GET).

Inputs: For a given NUTS region g: fixed process $N_{x,g}$ with events (t_i, u_i); tested process $N_{y,g}$ with events (s_j, u_j); seasonal intensities $\hat{\lambda}_x, \hat{\lambda}_y$; set of radii $\mathcal{R}$ (days); simulation budget n_{sim}; GET option *alternative* ("two.sided", "greater", "less"); reference centring (symmetric: $2r$, directional: r).

Outputs: Global rank envelope over $r \in \mathcal{R}$ and GET p-value.

♯ *Observed curve.*
Compute $\hat{K}^{\text{obs}}(\cdot)$ using Algorithm B5.
♯ *Total observation length.*
Define $T_{\text{tot}} \leftarrow N_{\text{year}}\, T$.
for $b = 1$ to n_{sim} **do**
  ♯ *Year-conditional periodic translation of DOY coordinates.*
  for each calendar year $y = 1, \ldots, N_{\text{year}}$ **do**
    Draw shift $\Delta_y^{(b)} \sim \text{Unif}(0, 1)$
    For all events of $N_{y,g}$ in year y, set $u' \leftarrow (u + \Delta_y^{(b)}) \bmod 1$
  end for
  ♯ *Map translated u back to continuous day times, preserving years.*
  $s'_j \leftarrow (y_j - 1)\, T + \text{DOY}(u'_j)$, where $\text{DOY}(u) = 1 + \lfloor uT \rfloor$.
  ♯ *Simulated curve.*
  Compute $\hat{K}^{(b)}(\cdot)$ from $(N_{x,g},\ N_{y,g}^{(b)})$ using Algorithm B5.
end for
♯ *Centre curves for testing independence.*
For symmetric cross-K: use $\hat{K}(\cdot) - 2r$; for directional cross-K: use $\hat{K}(\cdot) - r$.
♯ *Apply GET rank envelope test and compute global p-value.*
Apply GET to the centred curves; reject independence if $p < \alpha$.
♯ *Interpret alternative: "greater" = attraction; "less" = inhibition.*

Appendix C: Simulation study for method validation

C1 Objectives and design

To evaluate the statistical properties of the proposed temporal independence test based on the yearly cross-K function, we conducted a dedicated simulation study. The objectives were (i) to assess type I error control under independence in the presence of strong seasonal non-homogeneity, and (ii) to evaluate the ability of the test to detect short-term temporal dependence between extreme-event processes under controlled alternatives.

All simulations were defined on a yearly temporal domain ($T = 365$ d). For each scenario, $N_{\mathrm{rep}} = 200$ independent replications were generated, and inference was performed using global envelope tests based on 499 Monte Carlo simulations per replication. The significance level was fixed at $\alpha = 0.05$.

C2 Simulated scenarios

Two classes of scenarios were considered.

C2.1 Independent processes (null hypothesis)

Pairs of independent inhomogeneous Poisson processes with pronounced seasonal structure were simulated. Two configurations were examined:

- distinct seasonal peaks for the two processes (e.g. winter versus summer activity),
- identical seasonal patterns for both processes.

These scenarios were used to assess type I error control, both when seasonality was ignored (homogeneous assumption) and when seasonal intensity correction was applied.

C2.2 Dependent processes (alternative hypotheses)

Several forms of short-term temporal dependence, representative of climate-extreme dynamics, were simulated:

- cross-excitation between processes,
- directional lagged dependence,
- short-range temporal inhibition,
- dependence induced by common latent shocks affecting both processes.

C3 Inference procedure

For each replication, the cross-K function was estimated at daily temporal lags up to $r = 10$ d, considering only interactions within the same calendar year. Global envelope tests were constructed using Monte Carlo simulations under the null hypothesis. Seasonal non-homogeneity was accounted for via kernel-based intensity estimation on the day-of-year domain and intensity-preserving translations.

C4 Main findings

The simulation study led to the following conclusions.

- When seasonality was ignored, independent processes with different seasonal patterns were systematically rejected, highlighting the necessity of accounting for seasonal non-homogeneity.
- When seasonal intensity correction was applied, the empirical type I error under independence was close to the nominal level. Rejection rates under independence ranged between approximately 5.5 % and 7.5 % across inhomogeneous scenarios, which is compatible with Monte Carlo variability for 200 replications.
- Under all dependent scenarios considered, the test exhibited very high power, with rejection rates close to 100 % for the simulated interaction strengths.
- Additional experiments showed that the ability to detect dependence strongly depends on the number of events per year, emphasizing the role of sample size when interpreting results for rare extremes.

Overall, these simulations indicate that the proposed methodology reliably distinguishes independence from short-term temporal dependence in the presence of strong seasonal structure, provided that seasonal non-homogeneity is properly accounted for.

Code and data availability. All meteorological data used in this study are derived from the ERA5 reanalysis and accessed via the Copernicus Climate Data Store. These data are publicly available and can be obtained directly from https://doi.org/10.24381/cds.4991cf48 (Copernicus Climate Change Service, 2004).

All scripts used for data download, preprocessing, event detection, and statistical analysis, including the implementation of point process methods and Global Envelope Tests, are openly available in a public Git repository. The repository also contains the code required to reproduce all figures and results presented in this study: https://doi.org/10.5281/zenodo.23919088 (Heranval, 2026).

Author contributions. AH: Conceptualization, Data curation, Formal analysis, Investigation, Methodology, Software, Validation, Visualization, Writing – original draft. DA, EG, TO: Conceptualization, Supervision, Project administration, Resources, Funding acquisition, Writing – review & editing.

Competing interests. The contact author has declared that none of the authors has any competing interests.

Disclaimer. Publisher's note: Copernicus Publications remains neutral with regard to jurisdictional claims made in the text, published maps, institutional affiliations, or any other geographical representation in this paper. The authors bear the ultimate responsibility for providing appropriate place names. Views expressed in the text are those of the authors and do not necessarily reflect the views of the publisher.

Acknowledgements. We thank the Copernicus Climate Change Services for making the ERA5 reanalyses available. We also thank the three anonymous reviewers, and the editor for their valuable feedback, which has helped improve the manuscript.

Financial support. This research has been supported by the Chaire Geolearning funded by Andra, BNP-Paribas, CCR and SCOR Foundation.

Review statement. This paper was edited by Reetam Majumder and reviewed by three anonymous referees.

References

Barton, Y., Giannakaki, P., von Waldow, H., Chevalier, C., Pfahl, S., and Martius, O.: Clustering of regional-scale extreme precipitation events in southern Switzerland, Mon. Weather Rev., 144, 347–369, https://doi.org/10.1175/MWR-D-15-0205.1, 2016.

Cebrián, A. C. and Asín, J.: Analyzing Dependence between Point Processes in Time Using IndTestPP, R J., 13, 444–460, https://doi.org/10.32614/rj-2021-049, 2021.

Cebrián, A. C., Abaurrea, J., and Asín, J.: Testing independence between two nonhomogeneous point processes in time, J. Stat. Comput. Sim., 90, 2878–2901, https://doi.org/10.1080/00949655.2020.1792471, 2020.

Coles, S.: An Introduction to Statistical Modeling of Extreme Values, Springer, https://doi.org/10.1007/978-1-4471-3675-0, 2001.

Copernicus Climate Change Service: ERA5 post-processed daily statistics on single levels from 1940 to present, Climate Data Store [data set], https://doi.org/10.24381/cds.4991cf48, 2024.

Daley, D. J. and Vere-Jones, D.: An introduction to the theory of point processes: Volume I: Elementary theory and methods, Springer, https://doi.org/10.1111/j.1751-5823.2008.00054_18.x, 2003.

Davis, R. A. and Mikosch, T.: The extremogram: A correlogram for extreme events, Bernoulli, 15, 977–1009, https://doi.org/10.3150/09-bej213, 2009.

Davis, R. A. and Mikosch, T.: Measures of serial dependence for heavy-tailed time series, Extremes, 16, 295–320, https://doi.org/10.1007/s10687-016-0251-7, 2013.

Davison, A. C. and Smith, R. L.: Models for exceedances over high thresholds, J. R. Stat. Soc. B, 52, 393–442, https://doi.org/10.1111/j.2517-6161.1990.tb01796.x, 1990.

Diggle, P. J.: Statistical analysis of spatial and spatio-temporal point patterns, CRC Press, https://doi.org/10.1201/b15326, 2013.

Faranda, D., Messori, G., Coppola, E., Alberti, T., Vrac, M., Pons, F., Yiou, P., Saint Lu, M., Hisi, A. N. S., Brockmann, P., Dafis, S., Mengaldo, G., and Vautard, R.: ClimaMeter: contextualizing extreme weather in a changing climate, Weather Clim. Dynam., 5, 959–983, https://doi.org/10.5194/wcd-5-959-2024, 2024.

Faranda, D.: Enhancing public understanding of extreme weather events in a changing climate through ClimaMeter, Frontiers in Climate, https://doi.org/10.3389/fclim.2025.1688221, 2025.

Fischer, J., Groenemeijer, P., Holzer, A., Feldmann, M., Schröer, K., Battaglioli, F., Schielicke, L., Púčik, T., Antonescu, B., Gatzen, C., and TIM Partners: Invited perspectives: Thunderstorm intensification from mountains to plains, Nat. Hazards Earth Syst. Sci., 25, 2629–2656, https://doi.org/10.5194/nhess-25-2629-2025, 2025.

Gabriel, E., Opitz, T., and Bonneu, F.: Detecting and modeling multi-scale space-time structures: the case of wildfire occurrences, Journal de la Société Française de Statistique, 158, 86–105, http://www.numdam.org/item/JSFS_2017__158_3_86_0/ (last access: 18 February 2026), 2017.

Heranval, A.: Article—Idp-PP-Temporal, Zenodo [code], https://doi.org/10.5281/zenodo.23919088, 2026.

Hersbach, H., Bell, B., Berrisford, P., Biavati, G., Horányi, A., Muñoz Sabater, J., Nicolas, J., Peubey, C., Radu, R., Rozum, I., Schepers, D., Simmons, A., Soci, C., Dee, D., and Thépaut, J.-N.: ERA5 hourly data on single levels from 1940 to present, Climate Data Store [data set], https://doi.org/10.24381/cds.adbb2d47, 2023.

Hsing, T., Hüsler, J., and Leadbetter, M. R.: On the exceedance point process for a stationary sequence, Probab. Theory Rel., 78, 97–112, https://doi.org/10.1007/bf00718038, 1988.

Jacquemin, G., Allard, D., Freulon, X., and Vrac, M.: Return Period of Nonconcurrent Climate Compound Events: A Nonparametric Bivariate Generalized Pareto Approach, Environmetrics, 37, e70063, https://doi.org/10.1002/env.70063, 2026.

Kingman, J. F. C.: Poisson processes, vol. 3, Clarendon Press, https://doi.org/10.1093/oso/9780198536932.003.0005, 1992.

Koh, J., Pimont, F., Opitz, T., et al.: Spatiotemporal wildfire modeling through point processes with moderate and extreme marks, Ann. Appl. Stat., 17, 560–582, https://doi.org/10.1214/22-aoas1642, 2023.

Kohler, M. A. and Linsley, R. K.: Predicting the Runoff from Storm Rainfall, vol. 30, U.S. Department of Commerce, Weather Bureau, Washington, D.C., https://library.oarcloud.noaa.gov/noaa_documents.lib/NOAA_historic_documents/WB/Research_papers/WB_Research_Paper_34.pdf (last access: 28 October 2026), 1951.

Leonard, M., Westra, S., Phatak, A., Lambert, M., van den Hurk, B., McInnes, K., Risbey, J., Schuster, S., Jakob, D., and Stafford-Smith, M.: A compound event framework for understanding extreme impacts, WIRES Clim. Change, 5, 113–128, https://doi.org/10.1002/wcc.252, 2014.

Lewis, P. A. and Shedler, G. S.: Simulation of nonhomogeneous Poisson processes by thinning, Nav. Res. Logist. Q., 26, 403–413, https://doi.org/10.1002/nav.3800260304, 1979.

Lotwick, H. W. and Silverman, B. W.: Methods for analysing spatial processes of several types of points, J. R. Stat. Soc. B, 44, 406–413, https://doi.org/10.1111/j.2517-6161.1982.tb01221.x, 1982.

Moddemeyer, S., Sobhani, N., and Oztekin-Gunaydin, B.: Resilience for compounding and cascading events, National Academies Press, https://doi.org/10.17226/26659, 2022.

Myllymäki, M., Mrkvička, T., Grabarnik, P., Seijo, H., and Hahn, U.: Global envelope tests for spatial processes, J. R. Stat. Soc. B, 79, 381–404, https://doi.org/10.1111/rssb.12172, 2017.

Peng, R. D., Schoenberg, F. P., and Woods, J. A.: A space–time conditional intensity model for evaluating a wildfire hazard index, J. Am. Stat. Assoc., 100, 26–35, https://doi.org/10.1198/016214504000001763, 2005.

Pickands, J.: Statistical inference using extreme order statistics, Ann. Stat., 3, 119–131, https://doi.org/10.1214/aos/1176343003, 1975.

Pickands III, J.: The two-dimensional Poisson process and extremal processes, J. Appl. Probab., 8, 745–756, https://doi.org/10.1017/s0021900200114640, 1971.

Ripley, B. D.: The second-order analysis of stationary point processes, J. Appl. Probab., 13, 255–266, https://doi.org/10.2307/3212829, 1976.

Sharma, S. and Mujumdar, P.: Spatial synchrony, temporal clustering and dominant driver of streamflow droughts in Peninsular India, Environ. Res. Lett., 19, 074056, https://doi.org/10.1088/1748-9326/ad53e7, 2024.

Stocks, B. J., Lynham, T., Lawson, B., Alexander, M., Wagner, C. V., McAlpine, R., and Dube, D. E.: Canadian forest fire danger rating system: an overview, Forest. Chron., 65, 258–265, https://doi.org/10.5558/tfc65258-4, 1989.

Toreti, A., Cronie, O., and Zampieri, M.: Concurrent climate extremes in the key wheat producing regions of the world, Sci. Rep., 9, 5493, https://doi.org/10.1038/s41598-019-41932-5, 2019.

Tuel, A. and Martius, O.: A climatology of sub-seasonal temporal clustering of extreme precipitation in Switzerland and its links to extreme discharge, Nat. Hazards Earth Syst. Sci., 21, 2949–2972, https://doi.org/10.5194/nhess-21-2949-2021, 2021a.

Tuel, A. and Martius, O.: A global perspective on the sub-seasonal clustering of precipitation extremes, Weather and Climate Extremes, 33, 100348, https://doi.org/10.1016/j.wace.2021.100348, 2021b.

Tuel, A. and Martius, O.: Subseasonal temporal clustering of extreme precipitation in the Northern Hemisphere: Regionalization and physical drivers, J. Climate, 35, 3537–3555, https://doi.org/10.1175/JCLI-D-21-0562.1, 2022.

Weynants, M., Ji, C., Linscheid, N., Weber, U., Mahecha, M. D., and Gans, F.: Dheed: an ERA5 based global database of compound dry and hot extreme events from 1950 to 2023, Earth Syst. Sci. Data, 17, 6621–6645, https://doi.org/10.5194/essd-17-6621-2025, 2025.

Xi, D. D., Taylor, S. W., Woolford, D. G., and Dean, C.: Statistical models of key components of wildfire risk, Annu. Rev. Stat. Appl., 6, 197–222, https://doi.org/10.1146/annurev-statistics-031017-100450, 2019.

Zscheischler, J., Martius, O., Westra, S., Bevacqua, E., Raymond, C., Horton, R. M., van den Hurk, B., AghaKouchak, A., Jézéquel, A., Mahecha, M. D., Maraun, D., Ramos, A. M., Ridder, N. N., Thiery, W., and Vignotto, E.: A typology of compound weather and climate events, Nature Reviews Earth & Environment, 1, 333–347, https://doi.org/10.1038/s43017-020-0060-z, 2020.